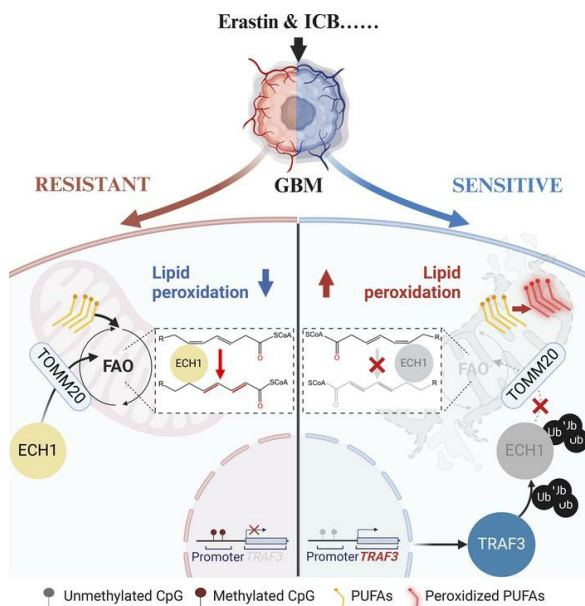# TRAF3 loss protects glioblastoma cells from lipid peroxidation and immune elimination via dysregulated lipid metabolism

Yu Zeng, … , Ye Song, Aidong Zhou

Research  In-Press Preview  Cell biology  Metabolism

## Graphical abstract

**TRAF3 Loss Protects Glioblastoma Cells from Lipid Peroxidation and Immune Elimination via Dysregulated Lipid Metabolism**

Yu Zeng[1,2], Liqian Zhao[3], Kunlin Zeng[1], Ziling Zhan[1,6], Zhengming Zhan[3], Shangbiao Li[1,4], Hongchao Zhan[1], Peng Chai[3], Cheng Xie[3], Shengfeng Ding[3], Yuxin Xie[1], Li Wang[1], Cuiying Li[1], Xiaoxia Chen[1], Daogang Guan[5], Enguang Bi[5], Jianyou Liao[6], Fan Deng[1*], Xiaochun Bai[1*], Ye Song[3,7*], Aidong Zhou[1,4,8*]

[1]Department of Cell Biology, School of Basic Medical Science, Southern Medical University, Guangzhou, 510515, China

[2]Department of Neurosurgery, Shanghai Ninth People's Hospital, Shanghai Jiao Tong University School of Medicine, Shanghai, 200011, China

[3]Department of Neurosurgery, Nanfang Hospital, Southern Medical University, 510515 Guangzhou, 510515, China

[4]Department of Radiation Oncology, Zhujiang Hospital, Southern Medical University, Guangzhou, 510280, China

[5]Department of Biochemistry and Molecular Biology, School of Basic Medical Sciences, Southern Medical University, Guangzhou, 510515, China

[6]Guangdong Provincial Key Laboratory of Malignant Tumor Epigenetics and Gene Regulation, Research Center of Medicine, Sun Yat-sen Memorial Hospital, Sun Yat-sen University, Guangzhou, 510120, China

[7]Department of Neurosurgery, Guangzhou Women and Children's Medical Center, Guangzhou Medical University, Guangdong Provincial Clinical Research Center for Child Health, Guangzhou, 510623, China

[8]Guangdong Province Key Laboratory of Molecular Tumor Pathology, School of Basic Medical Science, Southern Medical University, Guangzhou, 510515, China

**Authorship note**: AZ is the lead author. YZ, LZ and KZ contributed equally to this work.

**Address correspondence to**: Aidong Zhou, 1023 Shatai Road, Southern Medical University, Guangzhou 510515, China. Phone: 86.20.61648214; Email: aidern0927@smu.edu.cn. Or to: Ye Song, 1838 North Guangzhou Road, Department of Neurosurgery, Nanfang Hospital of Southern Medical University, Guangzhou 510515, China. Phone: 86.20.61641806; Email: Chinasongye@smu.edu.cn. Or to: Xiaochun Bai, 1023 Shatai Road, Southern Medical University, Guangzhou 510515, China. Phone: 86.20. 61648724; Email: baixc15@smu.edu.cn. Or to: Fan Deng, 1023 Shatai Road, Southern Medical University, Guangzhou 510515, China. Phone: 86.20. 61647073; Email: fandeng@smu.edu.cn.

**Running Title:** TRAF3 Loss Promotes Metabolism of PUFAs in GBM

**ABSTRACT**

Glioblastoma (GBM) is a highly aggressive form of brain tumor characterized by dysregulated metabolism. Increased fatty acid oxidation (FAO) protects tumor cells from lipid peroxidation-induced cell death, although the precise mechanisms involved remain unclear. Herein, we report that loss of tumor necrosis factor receptor-associated factor 3 (TRAF3) in GBM critically regulates lipid peroxidation and tumorigenesis by controlling the oxidation of polyunsaturated fatty acids (PUFAs). TRAF3 is frequently repressed in GBM due to promoter hypermethylation. TRAF3 interacts with enoyl-CoA hydratase 1 (ECH1), an enzyme catalyzing the isomerization of unsaturated fatty acids (UFAs), and mediates K63-linked ubiquitination of ECH1 at Lys214. ECH1 ubiquitination impedes TOMM20-dependent mitochondrial translocation of ECH1, which otherwise promotes the oxidation of UFAs, preferentially the PUFAs, and limits lipid peroxidation. Overexpression of TRAF3 enhances the sensitivity of GBM to ferroptosis and anti-PD-L1 immunotherapy in mice. Thus, the TRAF3-ECH1 axis plays a key role in the metabolism of PUFAs, and is crucial for lipid peroxidation damage and immune elimination in GBM.

**INTRODUCTION**

Glioblastoma (GBM), a highly aggressive type of brain cancer, is notorious for its resistance to treatments and poor prognosis, with a median overall survival time of only 15-18 months (1, 2). One hallmark of GBM is the reprogramming of cellular metabolism, allowing cancer cells to acquire increased energy and materials for their survival and growth (3, 4). Consequently, while GBM relies on glycolysis for energy, it exhibits a high degree of metabolic flexibility, enabling it to modulate its metabolic programs in response to the heterogeneity of the tumor microenvironment, including hypoxia, nutrient deprivation, and oxidative stress (5). In recent years, fatty acid oxidation (FAO) has gained significant attention as it critically contributes to the metabolic plasticity of GBM cells. FAO has been identified as an important source of ATP for highly glycolytic mesenchymal GBM cells to survive in nutrient-restricted conditions, and targeting FAO has emerged as a promising therapeutic approach for the treatment of GBM (6, 7).

Unsaturated fatty acids (UFAs) constitute an important source of lipids, which are required for the maintenance of membrane fluidity, signal transduction, and the lipid pool for β-oxidation (8). Fatty acid desaturases are enzymes that catalyze the addition of double carbon bonds to acyl chains, a vital process in the formation of mono- and poly-unsaturated FAs (MUFA and PUFA, respectively) (9). In recent years, the composition of membrane fatty acid, particularly the ratios of saturated fatty acids (SFAs), MUFAs and PUFAs, in regulating cell survival and lipotoxicity-related ferroptosis has been increasingly appreciated (10-12). However, while most studies

focused on the biosynthesis of UFAs, less attention has been paid to the regulation of UFA oxidation.

Tumor necrosis factor receptor (TNFR)-associated factors (TRAFs, TRAF1-7) constitute a family of intracellular signaling adaptors that interact with a range of receptors, including TNFR, Toll-like receptors, and interleukin receptors, playing crucial roles in innate immune signaling (13, 14). As a member of the TRAF family, TRAF3 is expressed in a variety of immune and non-immune cell types in mammals (15). TRAF3 knockout mice die soon after birth, indicating that TRAF3 possesses an essential and unique function that cannot be substituted by other TRAF members (16). Through its scaffolding function and E3 ubiquitin ligase activity, TRAF3 differentially modulates downstream signal cascades, such as activation of nuclear factor-κB (NF-κB), mitogen-activated protein kinase (MAPKs), and interferon regulatory factors (IRFs) (15, 17). Although the functions of TRAF3 in innate and adaptive immunity are well understood, its roles in tumor malignancy are less explored.

In this study, we investigated the prognostic value of the TRAF family members in cancer and identified TRAF3 as a member frequently repressed in GBM due to promoter hypermethylation. We revealed that TRAF3-mediated K63 ubiquitination of enoyl-CoA hydratase 1 (ECH1), an enzyme catalyzing the isomerization and metabolism of unsaturated fatty acids (18), impedes ECH1 mitochondrial translocation and critically regulates oxidation of PUFAs and lipid peroxidation. Exogenous expression of TRAF3 enhances the sensitivity of GBM to ferroptosis and effectively synergized with anti-PD-L1 therapy in an orthotopic GBM model, indicating a

promising therapeutic strategy for glioblastoma.

**RESULTS**

**Loss of *TRAF3* by promoter hypermethylation correlates with poor prognosis in glioma**

Although the TRAF family members as mediators of innate immune receptor signaling have been extensively investigated in myeloid cells (15), their roles in tumor malignancy are less explored. To comprehensively evaluate the prognostic significance of TRAF family members (TRAF1-7) in glioma, we first analyzed their expression patterns in the TCGA-glioma cohort. While high expression of other members was associated with poor prognosis, high-level *TRAF3* correlated with a significantly longer overall survival in glioma patients (Figure 1A). Interestingly, pan-cancer survival analysis demonstrated that glioma is the only cancer type in which *TRAF3* levels negatively correlated with patient survival (Supplemental Figure 1A), highlighting the distinctive role of TRAF3 in glioma compared to other tumor types. In multiple glioma datasets including TCGA-glioma, CGGA-glioma, and Fine brain dataset, a decrease of *TRAF3* level was observed as the tumor grade advances (Figure 1B). The reduction in *TRAF3* mRNA levels observed in GBM were further validated using the paired tumor and non-tumor brain tissues through quantitative RT-PCR (Figure 1C).

It has been previously documented that TRAF3 is predominantly expressed in glial cells, neuronal cells, and immune cells, including T and B cells (19). To examine the cell-type-specific expression pattern of *TRAF3* in glioma, we conducted a single-cell RNA-seq analysis based on publicly available datasets. In low-grade glioma (LGG), high *TRAF3* expression was observed in tumor cells, while moderate expression was

noted in myeloid cells (Figure 1D). In contrast, there was a notable reduction in *TRAF3* expression in tumor cells of GBM relative to those observed in LGG. Notably, although *TRAF3* expression is higher in myeloid and lymphoid cells in GBM compared to LGG (Figure 1D), the bulk RNA-seq results indicated lower overall *TRAF3* expression in GBM (Supplemental Figure 1B). This discrepancy suggests that *TRAF3* expression in tumor cells, rather than in non-tumor cells, is the primary determinant of the overall TRAF3 level in glioma. To elucidate the potential value of *TRAF3* in prognosis, we performed a multivariate Cox regression analysis involving *TRAF3* expression, MGMT methylation status, IDH mutation status, gender, grade, and age. The results demonstrated that among these factors, TRAF3 remained an independent predictor of a favorable prognosis in glioma, with elevated TRAF3 expression consistently correlating with improved survival outcomes, regardless of other clinical and genetic variables (Supplemental Figure 1C). These findings underscore the potential of TRAF3 as a valuable biomarker for glioma grading and indicate its specific involvement in glioma development.

Hypermethylation of the *TRAF3* promoter has been observed in cervical precancerous lesions compared with the healthy controls (20). Moreover, a recent study indicates that methylation sites frequently occur in CpG shores, regions approximately 0-2 kb away from the CpG islands in GBM (21). Consistent with this, our analysis revealed a higher probability of DNA methylation in the CpG shore within the *TRAF3* promoter region (Supplemental Figure 1D), implying that promoter methylation may serve as a critical mechanism for *TRAF3* expression. To validate our findings, we

performed bisulfite sequencing polymerase chain reaction (BSP-PCR) and methylation-specific PCR (MSP) assays to analyze the promoter methylation status of *TRAF3*. Our results demonstrated that the proportion of *TRAF3* promoter methylation was significantly higher in GBM tissues compared to the paired non-tumor brain tissues (Figure 1E and F). Furthermore, treatment with 5-Aza, a DNA methyltransferase inhibitor, resulted in a significant upregulation of *TRAF3* mRNA and protein levels in both patient-derived and commercially available GBM cell lines (Figure 1G and Supplemental Figure 1E). Accordingly, high *TRAF3* promoter methylation levels were observed in GBM cells (Supplemental Figure 1F). Consistent with the mRNA data, the TRAF3 protein level was markedly diminished in glioma specimens relative to the non-tumor tissues, and negatively correlated with glioma grade (Figure 1H). Taken together, these results demonstrate that TRAF3 is repressed in high-grade glioma by promoter hypermethylation, and decreased TRAF3 level correlates with poor survival of glioma patients.

**TRAF3 promotes ROS-related mitochondrial damage and inhibits GBM tumorigenesis**

To explore the functional implications of TRAF3 loss in glioma pathogenesis, we overexpressed TRAF3 in the patient-derived GBM0709 cells and then profiled gene expression by transcriptome sequencing (Supplemental Table 1). Gene Set Enrichment Analysis (GSEA) revealed a notable enrichment in the gene set associated with oxidative stress-induced senescence (Figure 2A, Supplemental Table 2). A panel of

genes related to oxidative stress exhibited a marked increase in expression following TRAF3 overexpression, including *TP53*, *MDM2*, and *FOS* (Figure 2B). Furthermore, a global alteration in the expression of histone genes, which have been demonstrated to be involved in oxidative stress-induced senescence, was also observed (22). Some of those genes were further validated by quantitative RT-PCR (Figure 2C).

Previous studies have indicated that TRAF3 plays a role in regulating oxidative status in cardiomyocytes (23), we therefore proceeded to investigate the effect of TRAF3 on the production of reactive oxygen species (ROS) and cellular senescence in GBM. The results demonstrated that both cellular and mitochondrial ROS were markedly elevated in GBM0709 and GBM0108 cells following TRAF3 overexpression (Figure 2D and E; Supplemental Figure 2A and B). Concurrently, the ratio of reduced glutathione (GSH) to oxidized glutathione (GSSG) (GSH/GSSG ratio) was decreased (Figure 2F and Supplemental Figure 2C). Given the close association between mitochondrial ROS levels and mitochondrial stability and function, we further examined the effect of TRAF3 on mitochondrial function. We observed a substantial decrease in mitochondrial membrane potential of GBM cells following TRAF3 overexpression as evidenced by JC-1 staining (Figure 2G and Supplemental Figure 2D). Transmission electron microscopy (TEM) images further demonstrated structural damage to the mitochondria, characterized by swollen cristae, upon TRAF3 overexpression (Figure 2H).

Senescence is a typical cellular phenomenon that is induced by the overproduction of cellular ROS and is characterized by irreversible cell cycle arrest (24). Consistent

10

with the results of transcriptome sequencing, we found that TRAF3 overexpression led to a significant increase of senescent cells and growth arrest of GBM cells, which was reversed by the addition of exogenous glutathione ethyl ester (GSH-EE) (Figure 2I and J; Supplemental Figure 2E and F). Moreover, the expression of senescence markers, including Clusterin, p53, and p21, were markedly elevated following TRAF3 overexpression (Supplemental Figure 2G). Using an in vivo intracranial mouse model, we further explored the role of TRAF3 in GBM tumorigenesis. We found that TRAF3 overexpression substantially suppressed GBM tumorigenicity in vivo and prolonged the overall survival of mice bearing GBM0709 tumors (median survival duration of 29 days for Ctrl vs 46 days for oeTRAF3) and GBM0108 tumors (24 days vs 40 days) (Figure 2K and L). Immunostaining of mouse GBM tissues demonstrated that TRAF3 overexpression significantly decreased the levels of Ki-67, while the levels of 8-oxoguanine (8-oxoG), indicative of oxidative DNA damage, and β-gal were increased (Figure 2M and Supplemental Figure 2H). Together, these findings suggest that TRAF3-induced ROS production and mitochondrial damage inhibit GBM tumorigenesis.

**TRAF3 interacts with and ubiquitinates ECH1 at Lys214 through K63-linked ubiquitin chains**

To explore the underlying mechanism by which TRAF3 regulates oxidative mitochondrial damage, we sought to identify the interacting proteins of TRAF3. To this end, Flag-tagged TRAF3 expressed in U87MG cells was immunoprecipitated, and the

interacting proteins were identified through silver staining and mass spectrometry analysis (Supplemental Table 3). Among the identified proteins with high abundance, enoyl-CoA hydratase 1 (ECH1), an enzyme that catalyzes the isomerization of unsaturated fatty acids for subsequent oxidation (18, 25), was selected for further investigation (Figure 3A). The reciprocal cellular interaction between TRAF3 and ECH1 was confirmed in GBM cells following treatment with 5-Aza, and in HEK293T cells after expression of the exogenous tagged proteins (Figure 3B and Supplemental Figure 3A). To determine the specific protein region of ECH1 that mediates its interaction with TRAF3, we constructed plasmids expressing different truncation mutants of ECH1 (Figure 3C). Co-immunoprecipitation results revealed that the C-terminal region of ECH1 (amino acid 202 to 328) is indispensable for its interaction with TRAF3 (Figure 3C).

The TRAF family members have been extensively studied as E3 ligases for substrate recognition and ubiquitination, especially in antiviral innate immunity (26), although only a few TRAF3 ubiquitination targets have been identified. We next determined the effect of TRAF3 on ECH1 ubiquitination. We found that TRAF3 overexpression increased the ubiquitination level of ECH1 in HEK293T cells, and the result was confirmed in GBM cells (Figure 3D and Supplemental Figure 3B). Accordingly, depletion of TRAF3 in SW1783 cells, a LGG cell line with relatively high TRAF3 expression, resulted in a notable reduction in ECH1 ubiquitination (Supplemental Figure 3C). Notably, treatment with 5-Aza, which upregulated TRAF3 expression, increased ECH1 ubiquitination in GBM0108 cells, and this effect was

reversed by further silencing of TRAF3 (Figure 3E). Because TRAF3 mediates both K48- and K63-linked ubiquitination (27, 28), we next determined the chain preference of ECH1 ubiquitination by TRAF3. The results demonstrated that while the wild-type and the K63-mutant ubiquitin (Ubi-K63, K63 wide-type only) strongly induced ECH1 ubiquitination, the K48-mutant ubiquitin (Ubi-K48, K48 wide-type only) had no effect on ECH1 ubiquitination (Figure 3F), indicating that TRAF3 ubiquitinates ECH1 through K63-linked ubiquitin chains.

Molecular docking showed that Lys214 and Lys276 in the C-terminal of ECH1 were located at the interaction interface between ECH1 and TRAF3, with inter-atomic distances of 1.9 and 4.4 Å, respectively. These two residues were found to be conserved among different species (Figure 3G)(29), suggesting potential ubiquitination of the residues by TRAF3. Therefore, we mutated these two residues (Lys to Arg) individually and found that K214R almost abolished ECH1 ubiquitination by TRAF3, whereas K276R did not (Figure 3H and Supplemental Figure 3D). Moreover, in vitro ubiquitination assays using purified proteins showed that TRAF3 ubiquitinated wild-type ECH1 in a K63-linked manner, whereas the ECH1-K214R mutant was not ubiquitinated (Figure 3I). Importantly, as with other K63-linked ubiquitination mediated by the TRAF family (30), we found that overexpression of TRAF3 had no effect on the expression and stability of the ECH1 protein in GBM cells (Supplemental Figure 3E). Together, our findings indicate that TRAF3 preferentially ubiquitinates ECH1 through K63-linked ubiquitin chains at Lys214.

**TRAF3-mediated ubiquitination of ECH1 inhibits its interaction with TOMM20 and mitochondrial translocation**

While K48-linked ubiquitination typically results in protein degradation, K63-linked ubiquitination is primarily involved in the regulation of protein function and subcellular localization (30). Given that ECH1 is predominantly localized in mitochondria and involved in the metabolism of UFAs, we hypothesized that TRAF3-mediated K63 ubiquitination of ECH1 may regulate its mitochondrial translocation. In GBM0709 and GBM0108 cells, the majority of the ECH1 proteins were observed to localize to mitochondria (Figure 4A and Supplemental Figure 4A). TRAF3 overexpression resulted in an increase in the fraction of cytoplasmic ECH1 and a concomitant decrease of mitochondrial ECH1 (Figure 4A and Supplemental Figure 4A). These results were confirmed by immunostaining in GBM0709 and HEK293T cells (Figure 4B and Supplemental Figure 4B). Notably, overexpression of TRAF3 did not significantly impede the mitochondrial translocation of ECH1-K214R (Figure 4C-E), indicating that TRAF3 inhibits ECH1 mitochondrial translocation in a K63-linked ubiquitination-dependent manner.

The translocase of the outer mitochondrial membrane (TOM) complex plays a vital role in transporting mitochondrial enzymes from the cytoplasm to the inner space of mitochondria. This complex is primarily composed of TOMM20, TOMM22, and TOMM40, with TOMM20 serving as a guide for the interaction between transported proteins and the TOM complex by binding to the mitochondrial leader sequences located in the N-terminus of the target proteins (31, 32). The BioGRID protein

14

interaction database indicated a potential interaction of ECH1 with TOMM20 and TOMM22 (Supplemental Figure 4C). The interaction between ECH1 and TOMM20 was subsequently confirmed by reciprocal immunoprecipitation and immunofluorescence assays (Figure 4F and Supplemental Figure 4D-F). Further, depletion of TOMM20 substantially impeded the translocation of ECH1 into the mitochondria (Figure 4G and H), indicating a requirement of TOMM20 for ECH1 mitochondrial translocation. We next investigated the impact of TRAF3-mediated K63 ubiquitination of ECH1 on its interaction with TOMM20. We revealed that TRAF3 overexpression notably disrupted the interaction between ECH1 and TOMM20 (Figure 4I). Importantly, while TRAF3 overexpression effectively impaired the association of TOMM20 and wild-type ECH1, it had no effect on the interaction between TOMM20 and ECH1-K214R (Figure 4J). Accordingly, while TRAF3 overexpression did not interrupt the translocation of ECH1-K214R into mitochondria (Figure 4D), concurrent TOMM20 depletion significantly impeded the mitochondrial translocation of ECH1-K214R (Figure 4K). Collectively, these results indicate that TRAF3-mediated K63 ubiquitination of ECH1 inhibits its interaction with TOMM20, thereby disrupting its mitochondrial translocation.

**Depletion of ECH1 promotes the accumulation of polyunsaturated fatty acids and lipid peroxidation**

Unlike SFAs that can directly undergo mitochondrial β-oxidation, UFAs require specific auxiliary enzymes to facilitate their complete oxidation (25, 33). ECH1 is one

such enzyme that catalyzes the cis-trans isomerization of UFAs with double bonds at odd-numbered positions along the carbon chain (Figure 5A), and has been proposed to play an important role in facilitating complete UFA metabolism (25, 33). Therefore, we investigated the role of ECH1 in mitochondrial oxidative metabolism of GBM cells. The expression level of *ECH1* is not significantly different in different grades of gliomas (Supplemental Figure 5A). As anticipated, depletion of ECH1 was found to significantly decrease both basal and maximal respiration capacity, as well as ATP production, as determined by oxygen consumption rate (OCR) analysis in GBM0709 and GBM0108 cells (Figure 5B-D and Supplemental Figure 5B-E). However, upon the addition of etomoxir (ETO), a CPT1 inhibitor that blocks the transport of long-chain fatty acids into mitochondria for FAO (34), ECH1 depletion did not further decreased basal and maximal respiration capacity or ATP production in GBM cells (Figure 5B-D and Supplemental Figure 5C-E). Similarly, although the supply of the PUFA LA-BSA stimulated mitochondrial respiration through FAO in GBM cells, no significant stimulation was observed following ECH1 depletion (Figure 5E-G and Supplemental Figure 5F-H). Moreover, the levels of acetyl-CoA, the end product of FAO, were markedly reduced following ECH1 depletion (Figure 5H and Supplemental Figure 5I). Thus, these results demonstrate that ECH1 is a pivotal regulator of FAO in GBM cells.

To gain insights into the metabolic alterations underlying the effect of ECH1 on FAO, we conducted a lipidomic analysis following ECH1 silencing (Supplemental Table 4). The results showed that depletion of ECH1 significantly promoted the accumulation of PUFAs, while decreasing the content of SFAs and MUFAs (Figure 5I).

Notably, ECH1 depletion resulted in a significant increase of several specific lipid species, including triglyceride (TG), phosphatidylglycerol (PG), and glycerolipids (GL) (Figure 5J and Supplemental Figure 5J). A comprehensive analysis of biosynthetic pathways based on lipidomic data (35), as conducted using BioPAN, further revealed an increase in the synthesis of cardiolipin (CL) and TG (Figure 5K and Supplemental Figure 5K). Consistently, the content of PUFAs was increased in CL and TG upon ECH1 silencing (Figure 5L and Supplemental Figure 5L). Specifically, the PUFA branches including C18:2, C20:2, and C18:3 were significantly increased in CL after ECH1 depletion (Figure 5M), indicating a preference of ECH1 in the metabolism of PUFAs in CL.

The accumulation of unmetabolized PUFAs usually triggers peroxidation (4). Moreover, CL, which is primarily composed of UFAs, is a characteristic lipid component of the mitochondrial membrane and is prone to peroxidation and oxidative damage, leading to mitochondrial dysfunction and collapse (36, 37). Therefore, we proceeded to investigate the effect of ECH1 depletion on lipid peroxidation. As anticipated, depleting ECH1 in GBM0709 and GBM0108 cells significantly upregulated the levels of malondialdehyde (MDA), a primary product of lipid peroxidation (Figure 5N and Supplemental Figure 5M). Moreover, BODIPY 581/591 staining also revealed a higher percentage of lipid peroxidation in GBM cells following ECH1 depletion (Figure 5O and Supplemental Figure 5N). Together, these results demonstrate that ECH1 depletion impedes the oxidation of PUFAs and stimulates lipid peroxidation in glioma cells.

**ECH1 depletion triggers ROS-related mitochondrial damage and inhibits GBM tumorigenesis**

Because UFAs are susceptible to oxidative damage, we hypothesized that accumulation of unmetabolized UFAs induced by ECH1 depletion may lead to mitochondrial failure. Consistent with the hypothesis, quantification of ROS production demonstrated that ECH1 depletion in GBM cells resulted in an increased level of cellular and mitochondrial ROS (Figure 6A and B; Supplemental Figure 6A and B), along with a decreased GSH/GSSG ratio (Figure 6C and Supplemental Figure 6C). Accordingly, ECH1 depletion decreased mitochondrial membrane potential as determined by JC-1 staining (Figure 6D and Supplemental Figure 6D). Further, TEM images revealed that ECH1 depletion led to damaged mitochondrial with darker matrices and swollen cristae (Figure 6E). Thus, these results indicate that ECH1 depletion promotes ROS-induced mitochondrial damage.

We next explored the role of ECH1 in cell growth and GBM tumorigenesis. As with TRAF3 overexpression, depletion of ECH1 reduced the levels of Clusterin, p53 and p21 in GBM cells, and these effects were reversed by GSH-EE (Supplemental Figure 6F). Accordingly, ECH1 depletion significantly induced cellular senescence and inhibited cell viability and colony formation of GBM cells, which were all reversed by treatment with GSH-EE (Figure 6F and G; Supplemental Figure 6E). In an orthotopic xenograft GBM model, ECH1 depletion in GBM0709 and GBM0108 cells resulted in a significant inhibition of tumor growth (Figure 6H) and a considerable prolongation

of the survival time of GBM-bearing mice (Figure 6I). In the mouse GBM tissues, ECH1 depletion was associated with a notable decline in Ki-67 expression compared to the control group, accompanied by elevated levels of 8-oxoG, 4-hydroxynonenal (4-HNE), and β-gal staining, which are indicative of oxidative DNA, lipid damage, and cellular senescence, respectively (Figure 6J and Supplemental Figure 6G). Taken together, these findings provide compelling evidence that ECH1 depletion triggers ROS-related mitochondrial damage and inhibits cell growth and GBM tumorigenesis.

**TRAF3 impedes FAO and induces lipid peroxidation through ubiquitination of ECH1**

We next determined whether TRAF3 regulates FAO and lipid peroxidation through the ubiquitination of ECH1. To this end, we first conducted a lipidomic analysis to examine the changes of lipid metabolism following TRAF3 overexpression. The results demonstrated that TRAF3 overexpression led to a reduction in the levels of SFAs and MUFAs and an increase in the accumulation of PUFAs (Figure 7A and Supplemental Table 5), which was consistent with the effect observed with ECH1 knockdown. Additionally, an increase in the levels of CL was observed following TRAF3 overexpression (Figure 7B), as well as an elevated proportion of PUFAs and MUFAs in the CL branch (Figure 7C). Notably, while overexpression of the wild-type ECH1 had no effect or a modest reversal of the effects of TRAF3 overexpression on PUFA levels, overexpression of ECH1-K214R substantially decreased the proportion of PUFAs caused by TRAF3 overexpression (Figure 7Aand C).

We proceeded to assess the impact of TAFR3-mediated ECH1 ubiquitination on mitochondrial respiration. Our findings revealed that TRAF3 overexpression markedly reduced mitochondrial respiration (Figure 7D-F and Supplemental Figure 7A-C), similar to the effect observed with ECH1 knockdown. Further analysis demonstrated that the reconstitution of wild-type ECH1 expression in GBM cells only marginally rescued the inhibitory effect of TRAF3 overexpression on the basal and maximal respiration capacity, as well as ATP production (Figure 7D-F and Supplemental Figure 7A-C). However, ECH1-K214R almost completely restored the oxidation capacity of GBM cells that was repressed by TRAF3 overexpression (Figure 7D-F and Supplemental Figure 7A-C). Notably, despite TRAF3's established role in inhibiting the NF-κB pathway in glioma, restoring the alternative NF-κB pathway by expressing MAP3K14 did not rescue the effect of TRAF3 overexpression on the oxidation capacity of GBM cells (Supplemental Figure 7D-G). This indicates that TRAF3 regulates glioma metabolism independently of the NF-κB pathway. Consistently, compared to wild-type ECH1, overexpression of ECH1-K214R was significantly more potent to upregulate the level of acetyl-CoA that was suppressed by TRAF3 overexpression (Figure 7G and Supplemental Figure 7H). Moreover, while wild-type ECH1 only slightly reversed the effect of TRAF3 overexpression on cellular and mitochondrial ROS levels, GSH/GSSG ratios, and MDA levels, ECH1-K214R significantly reversed those effects induced by TRAF3 overexpression (Figure 7H-K and Supplemental Figure 7I-L). In accordance with these findings, overexpression of ECH1-K214R, but not wild-type ECH1, substantially rescued GBM cells from growth arrest caused by TRAF3 overexpression

(Figure 7L and Supplemental Figure 7M).

In an orthotopic GBM model, we observed that reconstituted expression of ECH1-K214R in GBM cells with TRAF3 overexpression was more potent in promoting GBM growth compared to the wild-type ECH1, and accordingly markedly shorten the survival time of GBM0709 GBM-bearing mice (medium survival duration of 38 days in oeTRAF3+ECH1-WT versus 25 days in oeTRAF3+ECH1-K214R) (Figure 7M-O). In mouse GBM tissues, ECH1-K214R, but not wild-type ECH1, was observed to significantly elevate the levels of Ki-67, while concomitantly reducing the levels of 8-oxoG, and 4-HNE, which were affected by TRAF3 overexpression (Figure 7M). Collectively, these results demonstrate that TRAF3 inhibits FAO and promotes lipid peroxidation through the ubiquitination of ECH1.

**TRAF3 overexpression sensitizes GBM to ferroptosis and anti-PD-L1 therapy**

Accumulation of PUFAs and lipid peroxidation are hallmarks of ferroptosis (38). Therefore, we next investigated the role of TRAF3 in GBM cell ferroptosis. As anticipated, TRAF3 overexpression substantially enhanced erastin-induced ferroptosis in GBM0709 cells (IC50=18.35 μM in control vs 4.01 μM in TRAF3 overexpression group), GBM0108 cells (19.56 μM vs 8.66 μM), and U87MG cells (7.27 μM vs 3.76 μM) (Figure 8A and Supplemental Figure 8A). However, treatment with Ferrostatin, a ferroptosis inhibitor, did not rescue the growth inhibition effect caused by TRAF3 overexpression (Supplemental Figure 8B), indicating that TRAF3 sensitizes GBM cells to ferroptosis rather than directly inducing it. Consistently, in an orthotopic GBM model

using the erastin-resistant GBM0108 cells, erastin treatment alone did not significantly

promote lipid peroxidation and cell death in the tumors, and the GBM-bearing mice did

not benefit from erastin treatment (22 days in Ctrl vs 26 days in Erastin) (Figure 8B-D).

However, in the TRAF3 overexpression group, concomitant erastin treatment

substantially induced lipid peroxidation and cell death in the tumors. This combination

significantly inhibited tumor growth and prolonged the overall survival of GBM-

bearing mice (22 days in Ctrl vs 45 days in oeTRAF3 plus Erastin) (Figure 8B-D).

It has been reported that CD8^{+} T cells mediate tumor cell killing primarily through

ferroptosis, and blocking T cell-induced tumor cell ferroptosis leads to resistance to

immune checkpoint inhibitor (ICI) therapy (39, 40). Therefore, we investigated the

effect of TRAF3 overexpression on CD8^{+} T cells-mediated cell cytotoxicity. To this end,

GBM cells were co-cultured with activated CD8^{+} T cells at varying effector-to-target

(E:T) ratios. As we expected, while the cell viabilities decreased with increasing E-T

ratios, GBM cells expressing TRAF3 were more susceptible to CD8^{+} T cell-mediated

killing in comparison to the control group (Figure 8E and Supplemental Figure 8C).

Notably, the proportion of GZMB^{+} cells in the CD8^{+} T cell population was not

obviously altered between the control and TRAF3 overexpression groups

(Supplemental Figure 8D and E), suggesting that TRAF3 overexpression in GBM cells

did not affect the cytotoxicity of CD8^{+} T cells, but rather the susceptibility of tumor

cells to T cells. Further investigation using PI/calcein-AM staining substantiated that

ferrostatin treatment markedly impairs the cell killing of GBM cells by CD8^{+} T cells

induced by TRAF3 overexpression (Figure 8F and Supplemental Figure 8F). These

findings indicate that TRAF3 renders GBM cells susceptible to T cell killing by enhancing ferroptosis sensitivity.

To investigate the impact of TRAF3 overexpression on anti-PD-L1 immunotherapy, we established an orthotopic xenograft GBM model using mouse CT-2A and GL261 GBM cells, respectively (Figure 8G and Supplemental Figure 8G and H). Consistent with the in vitro assays, anti-PD-L1 treatment alone activated the anti-tumor CD8$^+$ T cell response, yet did not significantly induce tumor cell death and inhibit tumor growth (Figure 8H-J and Supplemental Figure 8H-L). In contrast, in the TRAF3 overexpression group, concomitant anti-PD-L1 treatment not only increased the population of cytolytic CD8$^+$ T cells but also significantly induced lipid peroxidation and cell death in mouse tumors (Figure 8H-J and Supplemental Figure 8H-L). As a result, the combination of PD-L1 blockade and TRAF3 overexpression significantly reduced the tumor burden and prolonged the survival of CT-2A GBM-bearing mice (23 days in PD-L1 mAb vs 40 days in PD-L1 mAb plus oeTRAF3) (Figure 8H-J). Similar outcomes were also observed in the GL261 GBM-bearing mice (20.5 days in PD-L1 mAb vs 45.5 days in PD-L1 mAb plus oeTRAF3) (Supplemental Figure 8M). Notably, the combined therapeutic effect was eliminated when the GL261 GBM-bearing mice were depleted of CD8$^+$ T cells (45.5 days in oeTRAF3 plus PD-L1 mAb vs 37 days in oeTRAF3 plus PD-L1 mAb and CD8α mAb) (Supplemental Figure 8M). Taken together, these findings provide compelling evidence that TRAF3-induced lipid peroxidation enhances the susceptibility of GBM cells to ferroptosis-inducing agents and anti-PD-L1 immunotherapy, suggesting a promising therapeutic strategy for

glioblastoma.

**DISCUSSION**

Dysregulation of lipid metabolism is a hallmark of cancer. Tumor cells utilize fatty acid to provide the necessary energy and building blocks for sustained tumor growth and to prevent potential lipotoxicity caused by the accumulation of unmetabolized UFAs, although the underlying mechanism remains largely unknown. In the present study, we demonstrate that the loss of TRAF3 in GBM activates ECH1-mediated metabolism of PUFAs, thereby inhibiting lipid peroxidation and promoting tumor growth. Overexpression of TRAF3 in GBM cells induces the accumulation of unmetabolized PUFAs and peroxidation mitochondrial damage, leading to increased sensitivity of GBM to ferroptosis and anti-PD-L1 immunotherapy, which indicates a promising strategy for GBM treatment.

Compared to other tumors, GBM displays distinctive characteristics in lipid metabolism. Dysregulated expression of genes associated with lipid metabolism is frequent in GBM. These include enzymes responsible for fatty acid synthesis (12), FAO (41), lipid transporters (42), and regulatory proteins involved in lipid homeostasis (7). As a result, GBM cells exhibit unique lipid profiles compared to normal glial cells and other tumor types (43). Such altered lipid profiles can impact a number of crucial cellular processes, including cell signaling, membrane structure, and overall cellular function. GBM cells display an increased reliance on FAO as a source of energy. This heightened FAO activity enables GBM cells to meet their increased energy demands and survive in nutrient-depleted conditions, such as limited glucose and oxygen availability, which are commonly observed in the GBM microenvironment (5, 44).

25

Furthermore, GBM frequently exhibit augmented accumulation of lipid droplets, which serve as intracellular lipid storage sites (45). These lipid droplets function as energy reservoirs and building blocks for membrane synthesis, thereby facilitating the rapid proliferation and invasive behavior of GBM cells (45).

While the majority of research focuses on the energy production aspect of enhanced FAO in cancer, it is important to recognize that FAO plays a multitude of roles beyond ATP production. These include cataplerotic reactions that provide substrates for amino acids, nucleotide synthesis, and improved redox potential (41, 46-48). GBM cells have been observed to upregulate the FAO pathway as a protective mechanism against lipid peroxidation, particularly of UFAs, which are susceptible to oxidative damage due to the presence of double bonds (38, 43). By enhancing FAO, GBM cells can minimize the accumulation of UFAs and reduce lipid peroxidation, thereby promoting their survival and proliferation (38). The dependency of malignant cells on FAO may represent a distinctive metabolic vulnerability. For instance, the inhibition of medium-chain acyl-CoA dehydrogenase (MCAD) did not elicit cytotoxic or the antiproliferative effects in normal glial cells, but decreased MCAD function in GBM cells resulted in a toxic accumulation of lipids which triggers mitochondrial failure (38). In the present study, we made an intriguing observation that TRAF3 is specifically associated with favorable survival outcomes in glioma cohorts compared to other types of tumors. This finding suggests that the catabolism pattern of PUFAs under the control of the TRAF3-ECH1 axis may be specific to glioma, potentially due to the vulnerability of GBM to lipid peroxidation. The dysregulated lipid metabolism

in GBM, along with the specific role of TRAF3 in modulating PUFA catabolism through K63-linked ubiquitination of ECH1, highlight the importance of understanding the unique metabolic characteristics of GBM.

As a cytoplasmic adaptor of the TRAF family, TRAF3 functions as an important mediator of innate immune receptor signaling through its scaffolding function and E3 ubiquitin ligase activity in different immune cells, including B cells, T cells, and macrophages (15). Several studies have investigated the tumor suppressive functions of TRAF3 in tumors, including B-cell lymphoma and head and neck cancers (49, 50). An association study has also indicated that high promoter methylation of *TRAF3* correlates with the progression of cervical intraepithelial neoplasia (20). Moreover, TRAF3 deficiency has been reported to regulate metabolism reprogramming in B cells (51). TRAF3 is a multifaceted regulator with a range of mechanisms of action. Prior research has demonstrated that TRAF3 suppresses the alternative NF-κB pathways in glioma (52). Although NF-κB pathway inactivation has been demonstrated to significantly downregulate several enzymes involved in FAO, including Acyl-CoA dehydrogenase family member 9 (ACAD9), Acyl-CoA synthetase long-chain family member 4 (ACSL4), and Fatty acid desaturase 2 (FADS2) (53), our present study found that rescuing the alternative NF-κB pathway did not restore the decreased OCR caused by TRAF3 overexpression. This result suggests that TRAF3 regulates glioma metabolism through mechanisms that extend the NF-κB pathway. Furthermore, our findings indicate that while overexpression of the wild-type ECH1 did not significantly reverse the effect of TRAF3 overexpression on PUFAs accumulation, lipid metabolism,

27

and GBM growth, transfection of the K214R mutant ECH1 markedly reversed these effects. These findings provide compelling evidence that loss of TRAF3 critically regulates metabolic plasticity in glioma through the regulation of ECH1 ubiquitination.

Unlike SFAs that directly enter mitochondrial for β-oxidation, UFAs require specific enzymes to facilitate their complete oxidation. ECH1 is an essential enzyme catalyzing the isomerization of the 3,5-dienoyl-CoA substrate to 2,4-dienoyl-CoA, which is regarded as a crucial step in the reductase-dependent pathway because the 3,5-dienoyl-CoA substrate is a "dead end metabolite" that is exclusively metabolized by ECH1 (25, 33). Consistent with the potential function of ECH1 in lipid metabolism, our study revealed that depletion of ECH1 leads to impaired FAO, preferentially through accumulation of PUFAs in CL and TG, resulting in oxidative mitochondrial damage and cell growth arrest. These results highlight the importance of ECH1-mediated isomerization and metabolism of PUFAs in lipid peroxidation and GBM tumorigenesis. Notably, the mRNA levels of *ECH1* is not significantly changed between low grade glioma and GBM tumors (Supplemental Figure 5A). Thus, TRAF3-mediated K63 ubiquitination and mitochondrial translocation of ECH1 may play a vital role in regulating ECH1 activity and metabolic plasticity in GBM. Similarly, acetylation of enoyl-CoA hydratase, short chain 1 (ECHS1), another member of the enoyl-CoA hydratase family responsible for the second step of hydration of FAO, has been shown to impede its mitochondrial translocation and activity (54).

The responsiveness of tumor to immunotherapies is not only related to the cytotoxic activity of immune cells within the tumor microenvironment (TME), but also

to the susceptibility of tumor cells to immune cell killing. Ferroptosis is a distinct form of programmed cell death characterized by iron accumulation and phospholipid peroxidation, and has been proposed as a major type of cell death induced by immune cells-mediated cell killing, including CD8^{+} T cells and neutrophils (39, 55). The present study demonstrated that the overexpression of TRAF3 in GBM cells did not directly induce ferroptosis or the cytotoxicity of CD8^{+} T cells. However, TRAF3-induced accumulation of unmetabolized PUFAs and lipid peroxidation led to increased vulnerability of GBM cells to ferroptosis induced by CD8^{+} T cells, and sensitizes GBM to anti-PD-L1 immunotherapy. Therefore, the TRAF3-ECH1 axis-regulated PUFA metabolism controls the energy supply on the one hand, and modulates the vulnerability of tumor cell to T cell-mediated cell killing on the other hand. Combination approaches that simultaneously target cancer metabolism and unleash the power of immunotherapy hold promise for improving patient outcomes in cancer treatment.

While the present study yielded promising findings, several limitations warrant further investigation in future. First, although our study reveals that the TRAF3-ECH1 axis induces lipid peroxidation and subsequently increases the susceptibility of GBM cells to ferroptosis inducers, including anti-PD-L1 immunotherapy, direct mechanistic evidence linking lipid peroxidation with the efficacy of immunotherapy is required. Secondly, the direct impact of lipid accumulation on immune elimination of GBM cells in the context of TRAF3 overexpression was not investigated. Accordingly, further research is necessary to examine the effect of lipid metabolism products on immune cells. At last, the clinical application of manipulating the TRAF3-ECH1 axis is

confronted with several challenges, including the efficient delivery of genes, potential off-target effects, and the assurance of sustained expression levels. Recent advances in nanotechnology and material science have demonstrated the potential for developing efficient delivery systems for RNA and proteins targeting specific cells (56, 57). The insights gained from our study provide a foundation for future therapeutic strategies that leverage advanced delivery systems and combination treatments.

In conclusion, our study demonstrated that loss of TRAF3 in GBM induces mitochondrial translocation of ECH1 and oxidation of PUFAs, thereby inhibiting lipid peroxidation and promotes tumor growth. Our findings highlight a critical role of the TRAF3-ECH1 axis in the oxidation of PUFAs, and targeting the axis represents a promising strategy to repress GBM growth and enhance the vulnerability of GBM to immunotherapies.

**METHODS**

*Sex as a biological variable*. Clinical samples of both sexes were included in this study. Nude mice and C57BL/6J mice of both sexes were used in this study.

*Statistical analysis*. Statistical analysis was performed using Prism Software (GraphPad) or R software (R Foundation for Statistical Computing). Data are expressed as the means ± standard deviation (SD). For representative data, results were repeated at least three independent experiments. For quantitative data, the statistical test used is indicated in the Figure Legends. Statistical differences between two groups were analyzed by unpaired or paired, two-tailed Student's t-test. One-way ANOVA followed by Tukey's post-hoc test was used to compare differences between multiple groups. Statistical significance of survival between groups was analyzed by log-rank test. $P<0.05$ was considered as statistically significant.

*Study Approval.* All procedures for rodent experiments and the determination of end points of animals were performed in accordance with the guidelines and protocols provided by the Southern Medical University Institutional Animal Care and Use Committee. Anonymous archived human glioma specimens were obtained from Department of Neurosurgery of Nanfang Hospital of Southern Medical University (Guangzhou, China) under a protocol approved by the institutional review board. Written informed consent was obtained from all participants.

*Data availability.* The raw RNA-seq data of this study has been deposited in the GEO database at accession code GSE285922. Values for all data points in graphs are reported in the Supporting Data Values file. The data generated in this study are available upon request from the corresponding author.

**AUTHORS' CONTRIBUTIONS**

A. Z. and Y.Z. conceived the study. Y. Z., L.Z. and K.Z. designed and performed most of the experiments. Z.Z., P.C., C.X., S.D., Y.X., S.L., L.W., C. L. and X.C. assisted in some in vitro experiments. Z.Z. and H.Z. assisted in the bioinformatic analysis. D.G., E.B., J.L, F.D., X.B. and Y.S. provided tissue samples, reagents and conceptual advice. A.Z. and Y.Z. wrote and revised the manuscript. A. Z. supervised the study. All authors discussed the results and commented on the manuscript.

**ACKNOWLEDGMENTS**

## REFERENCES

1.	Dolecek TA, Propp JM, Stroup NE, and Kruchko C. CBTRUS statistical report: primary brain and central nervous system tumors diagnosed in the United States in 2005-2009. *Neuro Oncol.* 2012;14 Suppl 5(Suppl 5):v1-49.

2.	Stupp R, Hegi ME, Mason WP, van den Bent MJ, Taphoorn MJ, Janzer RC, et al. Effects of radiotherapy with concomitant and adjuvant temozolomide versus radiotherapy alone on survival in glioblastoma in a randomised phase III study: 5-year analysis of the EORTC-NCIC trial. *Lancet Oncol.* 2009;10(5):459-66.

3.	Shakya S, Gromovsky AD, Hale JS, Knudsen AM, Prager B, Wallace LC, et al. Altered lipid metabolism marks glioblastoma stem and non-stem cells in separate tumor niches. *Acta Neuropathol Commun.* 2021;9(1):101.

4.	Taib B, Aboussalah AM, Moniruzzaman M, Chen S, Haughey NJ, Kim SF, et al. Lipid accumulation and oxidation in glioblastoma multiforme. *Sci Rep.* 2019;9(1):19593.

5.	Bi JF, Chowdhry S, Wu SH, Zhang WJ, Masui K, and Mischel PS. Altered cellular metabolism in gliomas - an emerging landscape of actionable co-dependency targets. *Nature Reviews Cancer.* 2020;20(1):57-70.

6.	Miska J, and Chandel NS. Targeting fatty acid metabolism in glioblastoma. *J Clin Invest.* 2023;133(1).

7.	Cheng X, Geng F, Pan M, Wu X, Zhong Y, Wang C, et al. Targeting DGAT1 Ameliorates Glioblastoma by Increasing Fat Catabolism and Oxidative Stress. *Cell Metab.* 2020;32(2):229-42 e8.

8.	Hoy AJ, Nagarajan SR, and Butler LM. Tumour fatty acid metabolism in the context of therapy resistance and obesity. *Nat Rev Cancer.* 2021;21(12):753-66.

9.	Lee JM, Lee H, Kang S, and Park WJ. Fatty Acid Desaturases, Polyunsaturated Fatty Acid Regulation, and Biotechnological Advances. *Nutrients.* 2016;8(1).

10.	Zhao GY, Tan YY, Cardenas H, Vayngart D, Wang YN, Huang H, et al. Ovarian cancer cell fate regulation by the dynamics between saturated and unsaturated fatty acids. *Proceedings of the National Academy of Sciences of the United States of America.* 2022;119(41).

11.	Scott JS, Nassar ZD, Swinnen JV, and Butler LM. Monounsaturated Fatty Acids: Key Regulators of Cell Viability and Intracellular Signaling in Cancer. *Mol Cancer Res.* 2022;20(9):1354-64.

12.	Gimple RC, Kidwell RL, Kim LJY, Sun TQ, Gromovsky AD, Wu QL, et al. Glioma Stem Cell-Specific Superenhancer Promotes Polyunsaturated Fatty-Acid Synthesis to Support EGFR Signaling. *Cancer Discovery.* 2019;9(9):1248-67.

13.	So T. The immunological significance of tumor necrosis factor receptor-associated factors

(TRAFs). *Int Immunol.* 2021.

14.     Zhang X, Xiong T, Gao L, Wang Y, Liu L, Tian T, et al. Extracellular fibrinogen-binding protein released by intracellular Staphylococcus aureus suppresses host immunity by targeting TRAF3. *Nat Commun.* 2022;13(1):5493.

15.     Jung J, Gokhale S, and Xie P. TRAF3: A novel regulator of mitochondrial physiology and metabolic pathways in B lymphocytes. *Front Oncol.* 2023;13:1081253.

16.     Xu Y, Cheng G, and Baltimore D. Targeted disruption of TRAF3 leads to postnatal lethality and defective T-dependent immune responses. *Immunity.* 1996;5(5):407-15.

17.     Hornick EL, and Bishop GA. TRAF3: Guardian of T lymphocyte functions. *Front Immunol.* 2023;14:1129251.

18.     Liang X, Zhu D, and Schulz H. Delta3,5,7,Delta2,4,6-trienoyl-CoA isomerase, a novel enzyme that functions in the beta-oxidation of polyunsaturated fatty acids with conjugated double bonds. *J Biol Chem.* 1999;274(20):13830-5.

19.     Gissler MC, Stachon P, Wolf D, and Marchini T. The Role of Tumor Necrosis Factor Associated Factors (TRAFs) in Vascular Inflammation and Atherosclerosis. *Front Cardiovasc Med.* 2022;9:826630.

20.     Huang S, Li R, Huang X, Zheng S, Wang L, Wen Z, et al. Association Study Between Methylation in the Promoter Regions of cGAS, MAVS, and TRAF3 Genes and the Risk of Cervical Precancerous Lesions and Cervical Cancer in a Southern Chinese Population. *Front Genet.* 2019;10:1123.

21.     Johnson KC, Anderson KJ, Courtois ET, Gujar AD, Barthel FP, Varn FS, et al. Single-cell multimodal glioma analyses identify epigenetic regulators of cellular plasticity and environmental stress response. *Nat Genet.* 2021;53(10):1456-68.

22.     Contrepois K, Coudereau C, Benayoun BA, Schuler N, Roux PF, Bischof O, et al. Histone variant H2A.J accumulates in senescent cells and promotes inflammatory gene expression. *Nat Commun.* 2017;8:14995.

23.     Liu X, Zhang L, Qin H, Han X, Zhang Z, Zhang Z, et al. Inhibition of TRAF3 expression alleviates cardiac ischemia reperfusion (IR) injury: A mechanism involving in apoptosis, inflammation and oxidative stress. *Biochem Biophys Res Commun.* 2018;506(1):298-305.

24.     Huang W, Hickson LJ, Eirin A, Kirkland JL, and Lerman LO. Cellular senescence: the good, the bad and the unknown. *Nat Rev Nephrol.* 2022;18(10):611-27.

25.     Luo MJ, Smeland TE, Shoukry K, and Schulz H. Delta 3,5, delta 2,4-dienoyl-CoA isomerase from rat liver mitochondria. Purification and characterization of a new enzyme involved in the beta-oxidation of unsaturated fatty acids. *J Biol Chem.* 1994;269(4):2384-8.

26.     Arkee T, and Bishop GA. TRAF family molecules in T cells: Multiple receptors and functions. *J Leukoc Biol.* 2020;107(6):907-15.

27.     Shi JH, Ling C, Wang TT, Zhang LN, Liu WW, Qin Y, et al. TRK-fused gene (TFG) regulates

ULK1 stability via TRAF3-mediated ubiquitination and protects macrophages from LPS-induced pyroptosis. *Cell Death Dis.* 2022;13(1):93.

28. Siu KL, Yuen KS, Castano-Rodriguez C, Ye ZW, Yeung ML, Fung SY, et al. Severe acute respiratory syndrome coronavirus ORF3a protein activates the NLRP3 inflammasome by promoting TRAF3-dependent ubiquitination of ASC. *FASEB J.* 2019;33(8):8865-77.

29. Yan Y, Tao H, He J, and Huang SY. The HDOCK server for integrated protein-protein docking. *Nat Protoc.* 2020;15(5):1829-52.

30. Zhang X, Li CF, Zhang L, Wu CY, Han L, Jin G, et al. TRAF6 Restricts p53 Mitochondrial Translocation, Apoptosis, and Tumor Suppression. *Mol Cell.* 2016;64(4):803-14.

31. Saitoh T, Igura M, Obita T, Ose T, Kojima R, Maenaka K, et al. Tom20 recognizes mitochondrial presequences through dynamic equilibrium among multiple bound states. *EMBO J.* 2007;26(22):4777-87.

32. Yamamoto H, Itoh N, Kawano S, Yatsukawa Y, Momose T, Makio T, et al. Dual role of the receptor Tom20 in specificity and efficiency of protein import into mitochondria. *Proc Natl Acad Sci U S A.* 2011;108(1):91-6.

33. van Weeghel M, te Brinke H, van Lenthe H, Kulik W, Minkler PE, Stoll MS, et al. Functional redundancy of mitochondrial enoyl-CoA isomerases in the oxidation of unsaturated fatty acids. *FASEB J.* 2012;26(10):4316-26.

34. Duman C, Yaqubi K, Hoffmann A, Acikgoz AA, Korshunov A, Bendszus M, et al. Acyl-CoA-Binding Protein Drives Glioblastoma Tumorigenesis by Sustaining Fatty Acid Oxidation. *Cell Metab.* 2019;30(2):274-89 e5.

35. Gaud C, B CS, Nguyen A, Fedorova M, Ni Z, O'Donnell VB, et al. BioPAN: a web-based tool to explore mammalian lipidome metabolic pathways on LIPID MAPS. *F1000Res.* 2021;10:4.

36. Liu NK, Deng LX, Wang M, Lu QB, Wang C, Wu X, et al. Restoring mitochondrial cardiolipin homeostasis reduces cell death and promotes recovery after spinal cord injury. *Cell Death Dis.* 2022;13(12):1058.

37. Ikon N, and Ryan RO. Cardiolipin and mitochondrial cristae organization. *Biochim Biophys Acta Biomembr.* 2017;1859(6):1156-63.

38. Puca F, Yu F, Bartolacci C, Pettazzoni P, Carugo A, Huang-Hobbs E, et al. Medium-Chain Acyl-CoA Dehydrogenase Protects Mitochondria from Lipid Peroxidation in Glioblastoma. *Cancer Discov.* 2021;11(11):2904-23.

39. Wang W, Green M, Choi JE, Gijon M, Kennedy PD, Johnson JK, et al. CD8(+) T cells regulate tumour ferroptosis during cancer immunotherapy. *Nature.* 2019;569(7755):270-4.

40. Xu H, Ye D, Ren M, Zhang H, and Bi F. Ferroptosis in the tumor microenvironment: perspectives for immunotherapy. *Trends Mol Med.* 2021;27(9):856-67.

41. Kant S, Kesarwani P, Prabhu A, Graham SF, Buelow KL, Nakano I, et al. Enhanced fatty acid

oxidation provides glioblastoma cells metabolic plasticity to accommodate to its dynamic nutrient microenvironment. *Cell Death Dis.* 2020;11(4):253.

42.  Jiang N, Xie B, Xiao W, Fan M, Xu S, Duan Y, et al. Fatty acid oxidation fuels glioblastoma radioresistance with CD47-mediated immune evasion. *Nat Commun.* 2022;13(1):1511.

43.  Minami JK, Morrow D, Bayley NA, Fernandez EG, Salinas JJ, Tse C, et al. CDKN2A deletion remodels lipid metabolism to prime glioblastoma for ferroptosis. *Cancer Cell.* 2023;41(6):1048-60 e9.

44.  Badr CE, Silver DJ, Siebzehnrubl FA, and Deleyrolle LP. Metabolic heterogeneity and adaptability in brain tumors. *Cell Mol Life Sci.* 2020;77(24):5101-19.

45.  Wu X, Geng F, Cheng X, Guo Q, Zhong Y, Cloughesy TF, et al. Lipid Droplets Maintain Energy Homeostasis and Glioblastoma Growth via Autophagic Release of Stored Fatty Acids. *iScience.* 2020;23(10):101569.

46.  Carracedo A, Cantley LC, and Pandolfi PP. Cancer metabolism: fatty acid oxidation in the limelight. *Nat Rev Cancer.* 2013;13(4):227-32.

47.  Randall EC, Lopez BGC, Peng S, Regan MS, Abdelmoula WM, Basu SS, et al. Localized Metabolomic Gradients in Patient-Derived Xenograft Models of Glioblastoma. *Cancer Res.* 2020;80(6):1258-67.

48.  Schoors S, Bruning U, Missiaen R, Queiroz KC, Borgers G, Elia I, et al. Fatty acid carbon is essential for dNTP synthesis in endothelial cells. *Nature.* 2015;520(7546):192-7.

49.  Bushell KR, Kim Y, Chan FC, Ben-Neriah S, Jenks A, Alcaide M, et al. Genetic inactivation of TRAF3 in canine and human B-cell lymphoma. *Blood.* 2015;125(6):999-1005.

50.  Zhang J, Chen T, Yang X, Cheng H, Spath SS, Clavijo PE, et al. Attenuated TRAF3 Fosters Activation of Alternative NF-kappaB and Reduced Expression of Antiviral Interferon, TP53, and RB to Promote HPV-Positive Head and Neck Cancers. *Cancer Res.* 2018;78(16):4613-26.

51.  Mambetsariev N, Lin WW, Wallis AM, Stunz LL, and Bishop GA. TRAF3 deficiency promotes metabolic reprogramming in B cells. *Sci Rep.* 2016;6:35349.

52.  Cai X, Yang Y, Xia W, Kong H, Wang M, Fu W, et al. RIP2 promotes glioma cell growth by regulating TRAF3 and activating the NF-kappaB and p38 signaling pathways. *Oncol Rep.* 2018;39(6):2915-23.

53.  Heise N, De Silva NS, Silva K, Carette A, Simonetti G, Pasparakis M, et al. Germinal center B cell maintenance and differentiation are controlled by distinct NF-kappaB transcription factor subunits. *J Exp Med.* 2014;211(10):2103-18.

54.  Zhang YK, Qu YY, Lin Y, Wu XH, Chen HZ, Wang X, et al. Enoyl-CoA hydratase-1 regulates mTOR signaling and apoptosis by sensing nutrients. *Nat Commun.* 2017;8(1):464.

55.  Yee PP, Wei Y, Kim SY, Lu T, Chih SY, Lawson C, et al. Neutrophil-induced ferroptosis promotes tumor necrosis in glioblastoma progression. *Nat Commun.* 2020;11(1):5424.

56.     Abune L, and Wang Y. Affinity Hydrogels for Protein Delivery. *Trends Pharmacol Sci.* 2021;42(4):300-12.

57.     Zhong R, Talebian S, Mendes BB, Wallace G, Langer R, Conde J, et al. Hydrogels for RNA delivery. *Nat Mater.* 2023;22(7):818-31.

# FIGURES
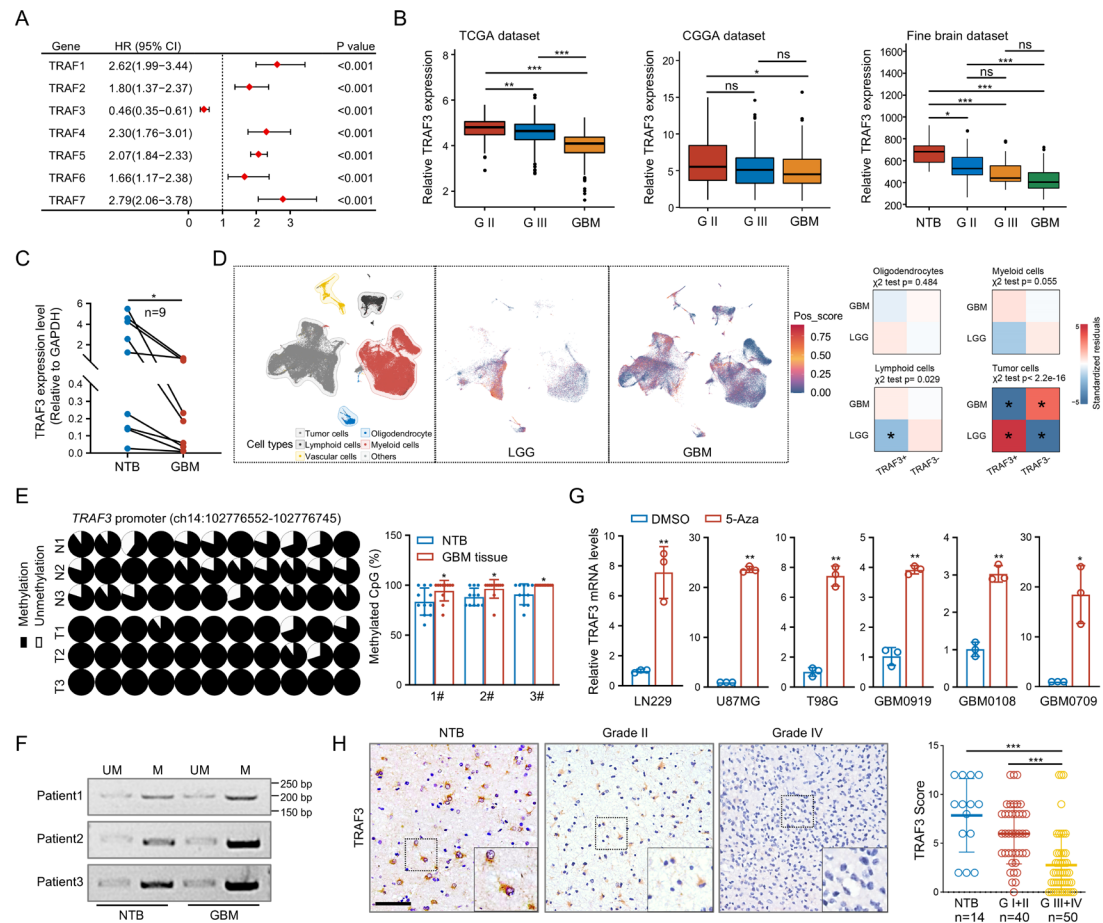


Figure 1. Loss of *TRAF3* by hypermethylation correlates with poor prognosis in glioma.

(A) Multivariate cox regression analysis of the TRAF family members in TCGA-glioma cohort.

(B) Analysis of *TRAF3* expression in glioma using TCGA, CGGA, and Fine brain dataset, respectively. ns, not significant. *P<0.05, **P<0.01, ***P<0.001.

(C) Analysis of *TRAF3* expression by qRT-PCR in glioblastoma (GBM) tissues and the paired non-tumor brain tissues (NTB) (n=9). *P<0.05.

**(D)** Analysis of single-cell RNA-seq data showing the expression of *TRAF3* across different cell types in low grade glioma (LGG) and GBM (SCP1985), respectively. The P values were indicated.

**(E)** Bisulfite sequencing polymerase chain reaction (BSP) was used to analyze the methylation of *TRAF3* promoter in GBM tissues and the paired NTB. The percentage of methylated CpG were statistically analyzed (mean ± SD, n=11 CpG sites for each tissue). *P<0.05.

**(F)** Methylation-specific PCR (MSP) analysis of three pairs of NTB and GBM tissues.

**(G)** GBM cells were treated with DMSO or 5-azacytidine (5-Aza), and the mRNA levels of *TRAF3* were analyzed by qRT-PCR. *GAPDH* was used as internal control. Values were normalized to DMSO (mean ±SD, n=3 independent experiments). *P<0.05, **P<0.01.

**(H)** TRAF3 protein in different grades of gliomas and the NTB tissues was analyzed by immunostaining. Representative images were shown. Scale bar, 200 μm. Staining of TRAF3 was scored on a scale of 0–12, and the expression scores of TRAF3 in grade III+IV were compared to those in NTB and grade I+II (n=14 NTB, n=40 grade I+II, and n=50 grade III+IV). ***P<0.001. Statistical analysis was performed using the one-way ANOVA with Tukey post hoc test (B and H), paired t-test (C), Chi-square test (D), or unpaired t-test (E and G).
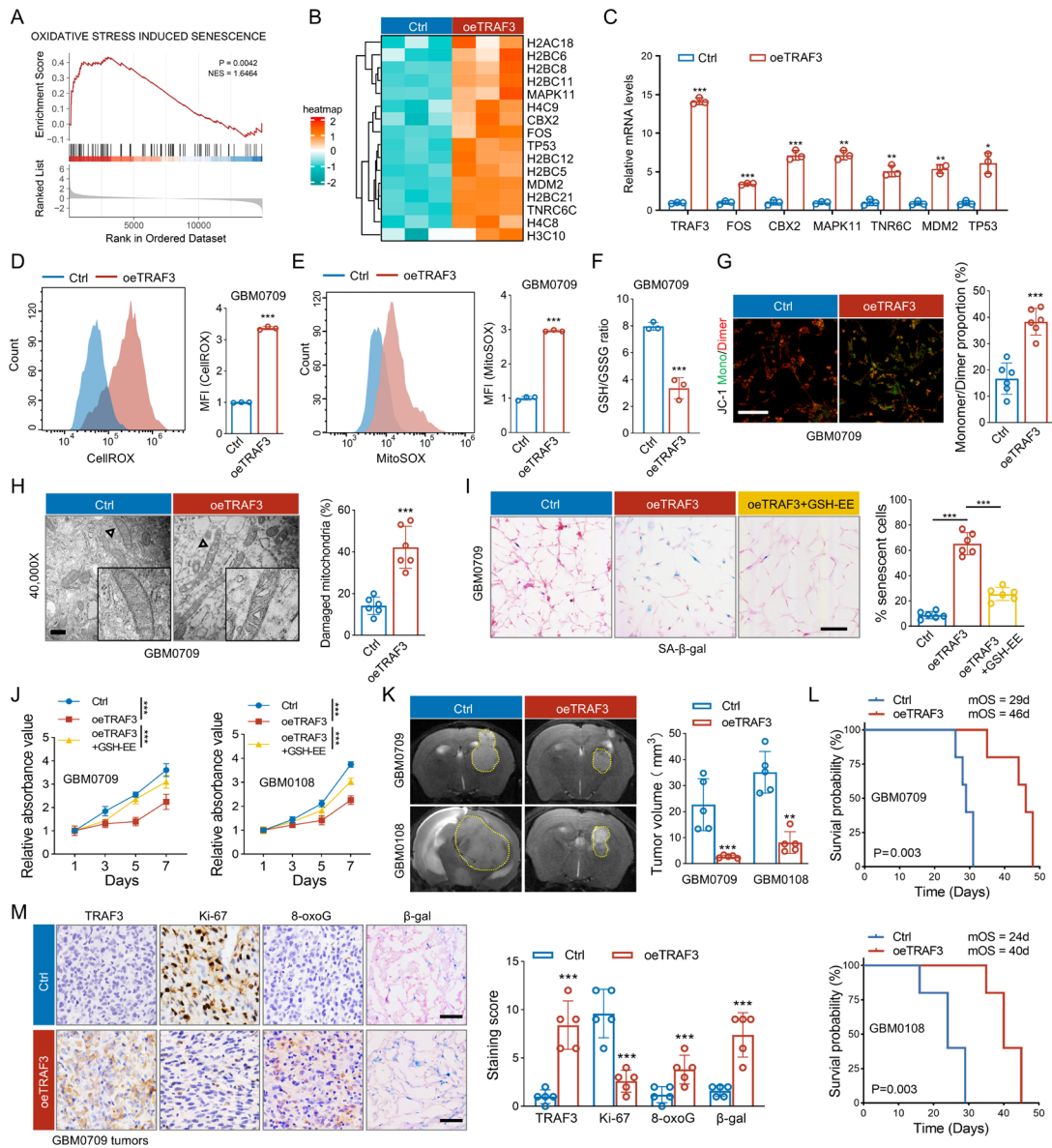
**Figure 2. TRAF3 promotes ROS-induced mitochondrial damage and inhibits GBM tumorigenesis.**

**(A)** Gene Set Enrichment Analysis (GSEA) to discern changes in expression levels of sets of genes after TRAF3 overexpression in GBM0709 cells.

**(B)** Heatmap shows the change of oxidative stress gene expression after TRAF3 overexpression in GBM0709 cells.

**(C)** The mRNA levels of selected genes in GBM0709 cells overexpressing TRAF3 were analyzed by qRT-PCR. *GAPDH* was used as internal control. Values were normalized to control (mean ± SD, n=3 independent experiments). *P<0.05, **P<0.01, ***P<0.001.

**(D** and **E)** The cellular (CellROX) and mitochondrial ROS (MitoSOX) levels of GBM0709 cells overexpressing TRAF3 were analyzed by flow cytometry. Representative flow cytometry plots were shown. The CellROX **(D)** and MitoSOX **(E)** levels were quantified as the median fluorescence intensity (MFI) (mean ± SD, n=3 independent experiments). ***P<0.001.

**(F)** The reduced glutathione/oxidized glutathione (GSH/GSSG) ratios in GBM0709 cells overexpressing TRAF3 were measured. Data were expressed mean ± SD of n=3 independent experiments. ***P<0.001.

**(G)** JC-1 staining of GBM0709 cells overexpressing TRAF3. Representative microscope images were shown, Scale bar, 100 μm. The monomer/dimer ratios of JC-1 were statistically analyzed (mean ± SD, n=6 randomly selected microscope fields). ***P<0.001.

**(H)** Transmission electron microscopy (TEM) images of mitochondria in GBM0709 cells overexpressing TRAF3 (magnification×40,000). Scale bar, 500 nm. The proportion of damaged mitochondria was statistically analyzed (mean ± SD, n=6 randomly selected microscope fields). ***P<0.001.

**(I)** GBM0709 cells overexpressing TRAF3 were treated with glutathione ethyl ester (GSH-EE) or not, and cells were then stained with SA-β-gal. Representative images

were shown. Scale bar, 100 μm. The percentages of β-gal positive cells were counted (mean ± SD, n=6 randomly selected microscope fields). \*\*\*P<0.001.

**(J)** GBM0709 and GBM0108 cells expressing TRAF3 were treated with GSH-EE or note, and cell viabilities in different time points were analyzed by CCK8. The absorbance values were normalized to control (mean ± SD, n=4 independent assays). \*\*\*P<0.001.

**(K)** GBM0709 or GBM0108 cells ($5\times10^5$ cells/mouse) stably expressing TRAF3 were intracranially injected into nude mice, and tumor growth was monitored by magnetic resonance imaging (MRI). Representative MRI images were shown. Tumor volumes of each group were statistically analyzed (mean ± SD, n=5 mice for each group). \*\*P<0.01, \*\*\*P<0.001.

**(L)** The survival of mice bearing GBM0709 and GBM0108 GBM tumors was evaluated (n=5 mice for each group, Kaplan-Meier model).

**(M)** Consecutive mouse GBM tissues derived from GBM0709 cells were stained with TRAF3, Ki-67, 8-oxoG, and β-gal, respectively. Scale bars, 100 μm. The staining scores in those two groups were compared with each other (mean ± SD, n=5 randomly selected microscope fields). \*\*\*P<0.001. Statistical analysis was performed using the unpaired t-test (C-H, K, and M), one-way ANOVA with Tukey post hoc test (I and J), or Log-rank test (L).
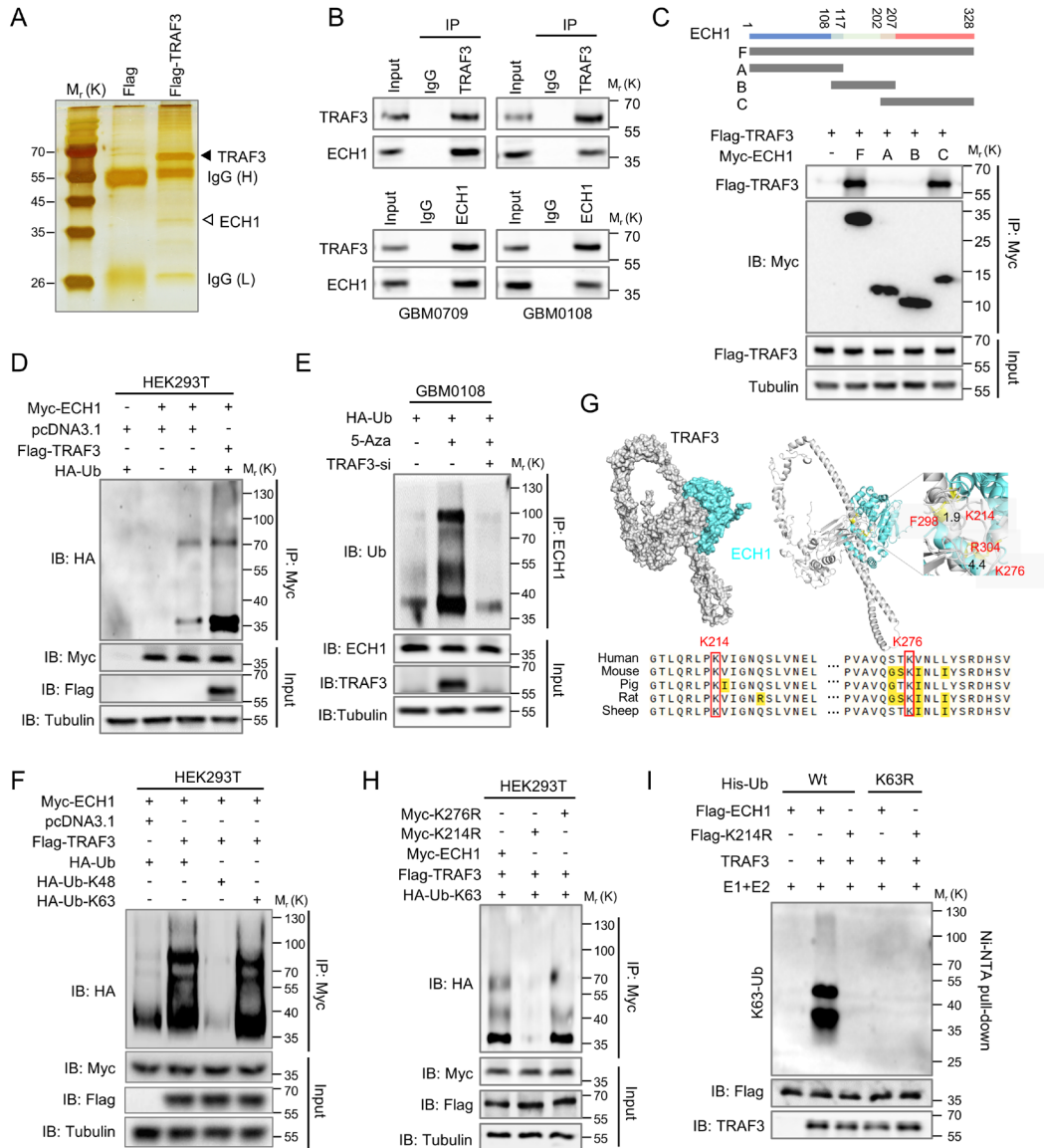
**Figure 3. TRAF3 interacts with ECH1 and promotes K63-linked ubiquitination of ECH1 at Lys214.**

**(A)** U87MG cells were transfected with Flag-TRAF3 and cell lysates were incubated with an anti-Flag-Tag antibody. The immunoprecipitated protein complexes were resolved on SDS-PAGE electrophoresis, and specific protein bands, identified by silver staining, were subjected to mass spectrometry analysis. The hollow arrow indicates the

ECH1 band identified by MS/MS. IgH and IgL indicate IgG heavy chain and light chain, respectively.

**(B)** Co-immunoprecipitation assays demonstrate the reciprocal interaction between TRAF3 and ECH1 in GBM0709 and GBM0108 cells after treatment with 5-Aza.

**(C)** Myc-tagged full-length ECH1 or deletion mutants were co-transfected with Flag-TRAF3 into HEK293T cells. Cell lysates were immunoprecipitated using an anti-Myc antibody, and the immunoprecipitates were analyzed by immunoblotting using the indicated antibodies.

**(D)** HEK293T cells were transfected with the Myc-ECH1, Flag-TRAF3, and HA-Ub plasmids. The cell lysates were incubated with an anti-Myc-tag antibody and then subjected to immunoblotting analysis.

**(E)** GBM0108 cells were transfected with TRAF3 siRNA and HA-Ub, and then were treated with 5-Aza. The cell lysates were immunoprecipitated with an anti-Myc antibody and then analyzed by immunoblotting.

**(F)** HEK293T cells were transfected with the indicated plasmids and then incubated with an anti-Myc-tag antibody. The resultant immunoprecipitates were analyzed by immunoblotting.

**(G)** The binding mode between TRAF3 and ECH1 was predicted by the HDOCK server. The protein tertiary structures for TRAF3 and ECH1 were retrieved from the Alphafold database. Yellow dashed lines indicate possible interactions, and residues highlighted in red indicate potential residues mediating protein-protein interactions. The inter-atomic distances between TRAF3 and ECH1 were indicated.

**(H)** HEK293T cells were transfected with Flag-TRAF3, HA-Ub-K63, and Myc-ECH1 or each of the ECH1 mutants (K214R or K276R). The cell lysates were immunoprecipitated with an anti-Myc antibody and then analyzed by immunoblotting.

**(I)** In vitro ubiquitination assay using the indicated purified proteins in the presence of E1, E2 enzymes, and $Mg^{2+}$-ATP (10 mM) in the ubiquitination reaction buffer. The reaction mixtures were purified by Ni-NTA beads, and the eluted proteins were analyzed by immunoblotting.
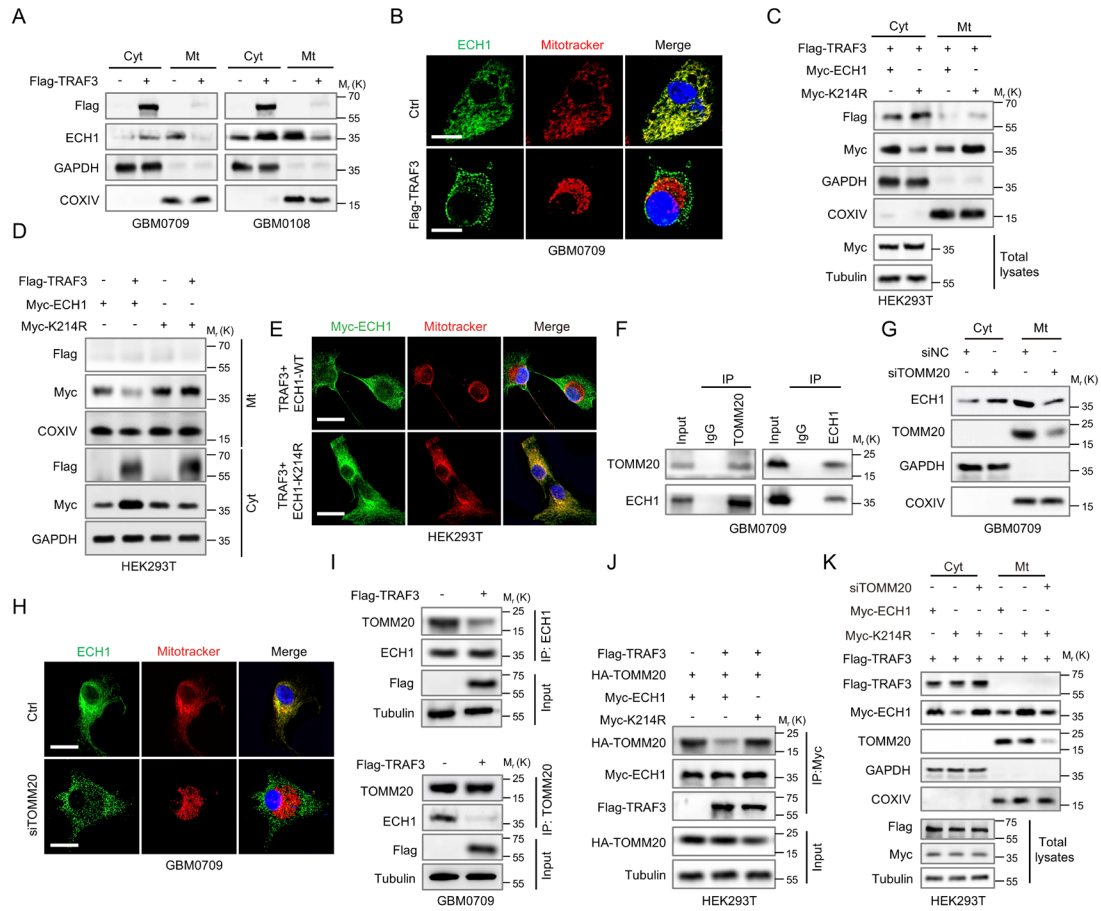
**Figure 4. TRAF3-mediated ubiquitination of ECH1 inhibits its mitochondrial translocation.**

**(A)** GBM0709 and GBM0108 cells were transfected with Flag-TRAF3 or control plasmid, and the cytosolic and mitochondrial protein fractions were isolated and then were subjected into immunostaining using the indicated antibodies.

**(B)** Immunofluorescent (IF) assays demonstrate the subcellular location of ECH1 in GBM0709 cells transfected with Flag-TRAF3. Scale bar, 20 μm.

**(C)** The cytosolic and mitochondrial levels of ECH1-WT or ECH1-K214R in HEK293T cells expressing Flag-TRAF3 were evaluated by immunoblotting.

48

**(D)** HEK293T cells were transfected with TRAF3 and ECH1-WT or ECH1-K214R, and the cytosolic and mitochondrial levels of ECH1 were evaluated by. immunoblotting.

**(E)** HEK293T cells were transfected with TRAF3 and ECH1-WT or ECH1-K214R, and the subcellular location of ECH1 were detected by immunostaining. Scale bar, 20 μm.

**(F)** GBM0709 cell lysates were immunoprecipitated with an antibody against ECH1 or TOMM20, and the resultant immunoprecipitates were subjected to immunoblotting.

**(G)** GBM0709 cells were transfected with TOMM20 siRNA, and the cytosolic and mitochondrial protein fractions were subsequently analyzed by immunoblotting.

**(H)** GBM0709 cells were transfected with TOMM20 siRNA, and the subcellular location of ECH1 were analyzed by IF. Scale bar, 20 μm.

**(I)** GBM0709 cells were transfected with TRAF3, and cell lysates were incubated with an antibody against ECH1 or TOMM20 and then subjected to immunoblotting.

**(J)** HEK293T cells were transfected with Flag-TRAF3, HA-TOMM20, and ECH1-WT or ECH1-K214R, and cell lysates were immunoprecipitated with an anti-Myc-tag antibody and then analyzed by immunoblotting.

**(K)** HEK293T cells were transfected with Flag-TRAF3, TOMM20 siRNA, and ECH1-WT or ECH1-K214R, and the cytosolic and mitochondrial protein fractions were isolated and then analyzed by immunoblotting using the indicated antibody.
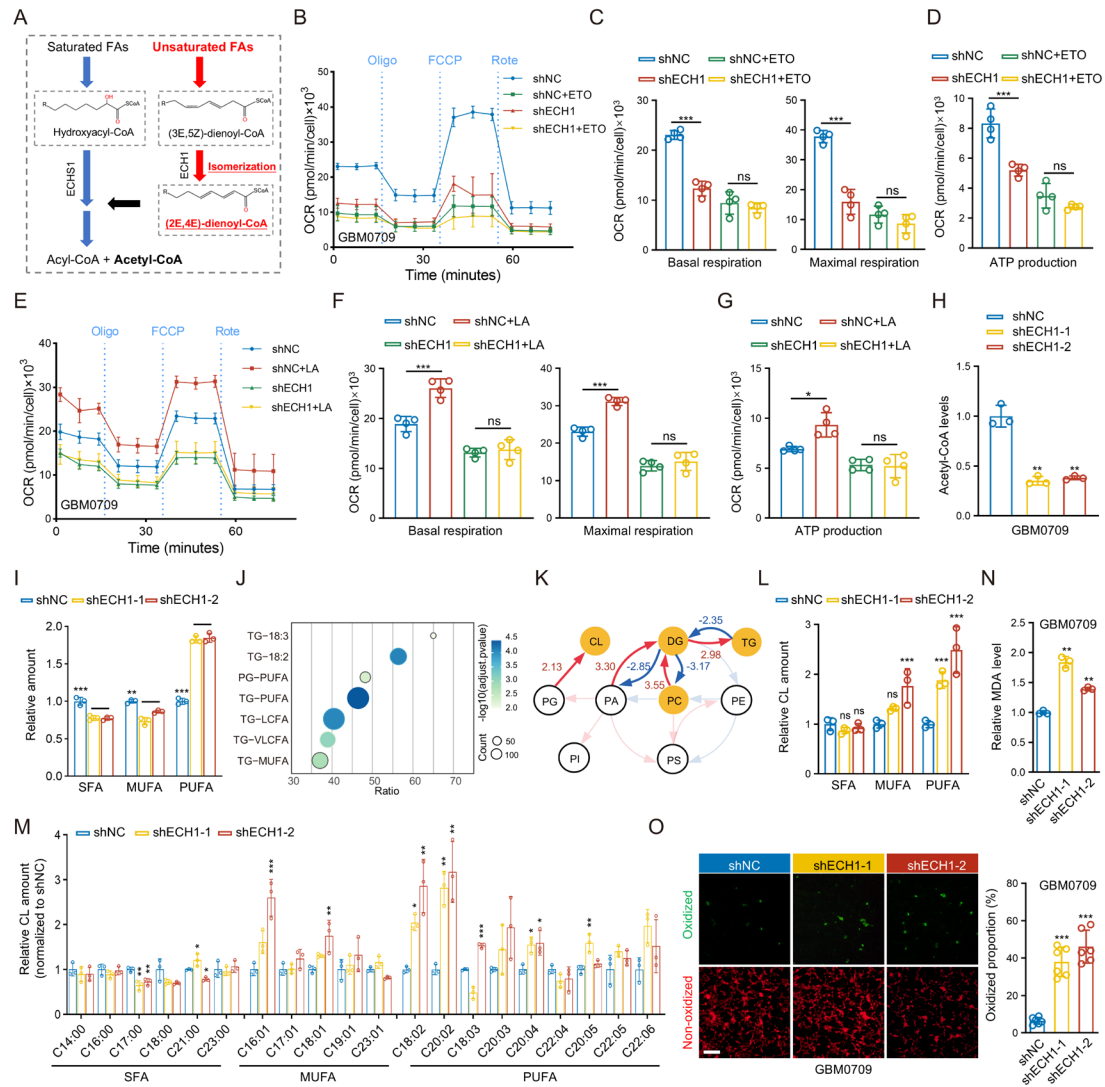
**Figure 5. Depletion of ECH1 induces accumulation of PUFAs and lipid peroxidation.**

**(A)** Scheme demonstrates the role of ECH1 in the metabolism of UFAs. ECH1 is an isomerase catalyzes the isomerization of a 3-trans, 5-cis dienoyl-CoA substrate to a 2-trans, 4-trans dienoyl-CoA product, which is required for subsequent oxidation of UFAs.

**(B)** GBM0709 cells stably expressing *ECH1* shRNA were treated with etomoxir (ETO) or not, and time series of oxygen consumption rate (OCR) was measured by Seahorse assays.

**(C)** Quantification of basal respiration and maximum respiration in GBM0709 cells.

**(D)** Quantification of mitochondrial ATP production in GBM0709 cells.

**(E)** GBM0709 cells stably expressing *ECH1* shRNA were treated with BSA conjugated linoleic Acid (LA-BSA) or not, and time series of oxygen consumption rate (OCR) was measured by Seahorse assays.

**(F)** Quantification of basal respiration and maximum respiration in GBM0709 cells.

**(G)** Quantification of mitochondrial ATP production in GBM0709 cells. From **(B)** to **(G)**, Data were expressed as mean ± SD of n=4 independent assays. ns, not significant. *P<0.05, ***P<0.001.

**(H)** Quantification of acetyl-CoA levels in GBM0709 cells expressing *ECH1* shRNAs compared to control shRNA (mean ± SD, n=3 independent experiments). **P<0.01.

**(I)** Lipidomic analysis demonstrated the relative content of SFAs, MUFAs, and PUFAs in GBM0709 cells expressing *ECH1* shRNAs compared to control shRNA (mean ± SD, n=3 independent experiments). **P<0.01, ***P<0.001.

**(J)** Enrichment analysis of upregulated lipid species in GBM0709 cells expressing shECH1-1 compared to control shRNA.

**(K)** Biosynthetic analysis of lipid species in GBM0709 cells expressing shECH1-1 compared to control shRNA.

**(L)** Analysis of the content of SFAs, MUFAs, and PUFAs in CL in GBM0709 cells

expressing *ECH1* shRNAs compared to control (mean ± SD, n=3 independent experiments). ns, not significant. ***P<0.001.

**(M)** Analysis of the specific fatty acid branches in (CL) in GBM0709 cells expressing *ECH1* shRNAs compared to control shRNA (mean ± SD, n=3 independent experiments). *P<0.05, **P<0.01, ***P<0.001.

**(N)** The level of malondialdehyde (MDA) was detected in GBM0709 cells expressing *ECH1* shRNAs. Data were expressed as mean ± SD of n=3 independent experiments. **P<0.01.

**(O)** BODIPY 581/591 staining of GBM0709 cells expressing *ECH1* shRNAs. Representative images were shown. Scale bars, 100 μm. The proportion of oxidized cells were calculated (mean ± SD, n=6 randomly selected microscope fields). ***P<0.001. Statistical analysis was performed using one-way ANOVA with Tukey post hoc test (C, D, F, G, H, I, L, M, N, and O).
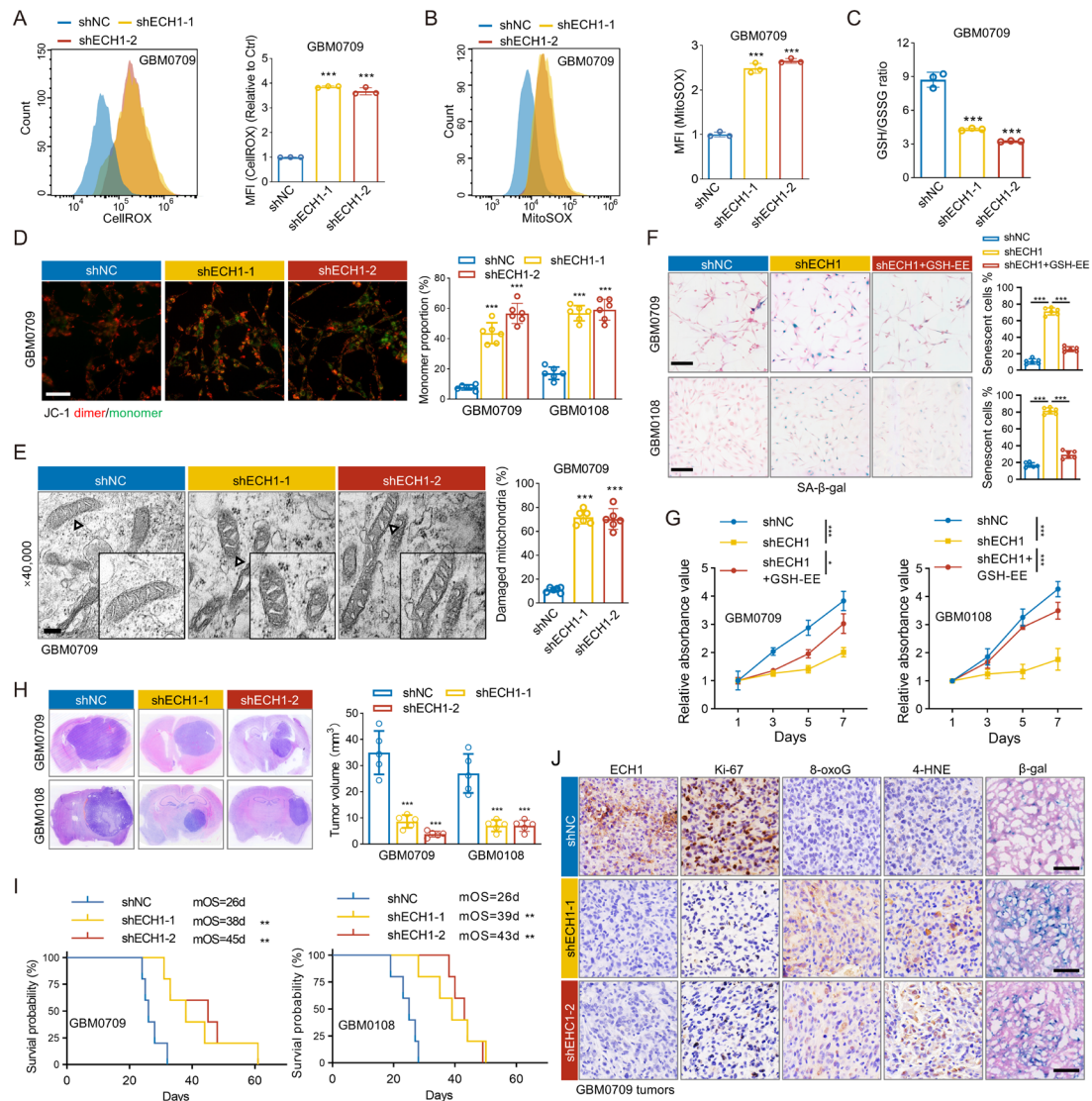
**Figure 6. ECH1 depletion triggers ROS-related mitochondrial damage and inhibits GBM tumorigenesis.**

(**A** and **B**) The CellROX (**A**) and MitoSOX (**B**) levels of GBM0709 cells stably expressing *ECH1* shRNAs were analyzed by flow cytometry. Representative flow cytometry plots were shown. The MFI was quantified (mean ± SD, n=3 independent experiments). ***P<0.001.

**(C)** GSH/GSSG ratios were evaluated in GBM0709 cells stably expressing *ECH1* shRNAs. Data were expressed as mean ± SD of n=3 independent experiments. ***P<0.001.

**(D)** JC-1 staining in GBM0709 cells stably expressing *ECH1* shRNAs. Representative images were shown. Scale bar, 100 μm. The proportions of JC-1 monomer (green) in each group were statistically analyzed (mean ± SD, n=6 randomly selected microscope fields). ***P<0.001.

**(E)** TEM images of mitochondria in GBM0709 cells stably expressing *ECH1* shRNAs (magnification×40,000). Scale bar, 500 nm. The proportion of damaged mitochondria was statistically analyzed (mean ± SD, n=6 randomly selected microscope fields). ***P<0.001.

**(F)** GBM0709 and GBM0108 cells stably expressing *ECH1* shRNA were treated with GSH or not, and cells were then stained with β-gal. Representative images were shown. Scale bars, 100 μm. The percentage of β-gal positive cells were counted (mean ± SD, n=6 randomly selected microscope fields). ***P<0.001.

**(G)** GBM0709 and GBM0108 cells stably expressing *ECH1* shRNA were treated with GSH or not, and cell viabilities were evaluated by CCK8. The absorbance values were normalized to control (mean ± SD, n=4 independent assays). *P<0.05, ***P<0.001.

**(H)** GBM0709 and GBM0108 cells stably expressing *ECH1* shRNAs were intracranially injected into nude mice. H&E-stained sections show representative tumor xenografts (left). Tumor volumes were calculated (mean ± SD, n=5 mice for each group). ***P<0.001.

**(I)** The survival of the GBM-bearing mice was evaluated (n=5 mice for each group, Kaplan-Meier model). **P<0.01.

**(J)** The mouse brain tissues derived from GBM0709 cells were stained with ECH1, Ki-67, 8-oxoG, 4-HNE, and SA-β-gal, respectively. Scale bars, 200 μm. Statistical analysis was performed using one-way ANOVA with Tukey post hoc test (A-H) or Log-rank test (I).
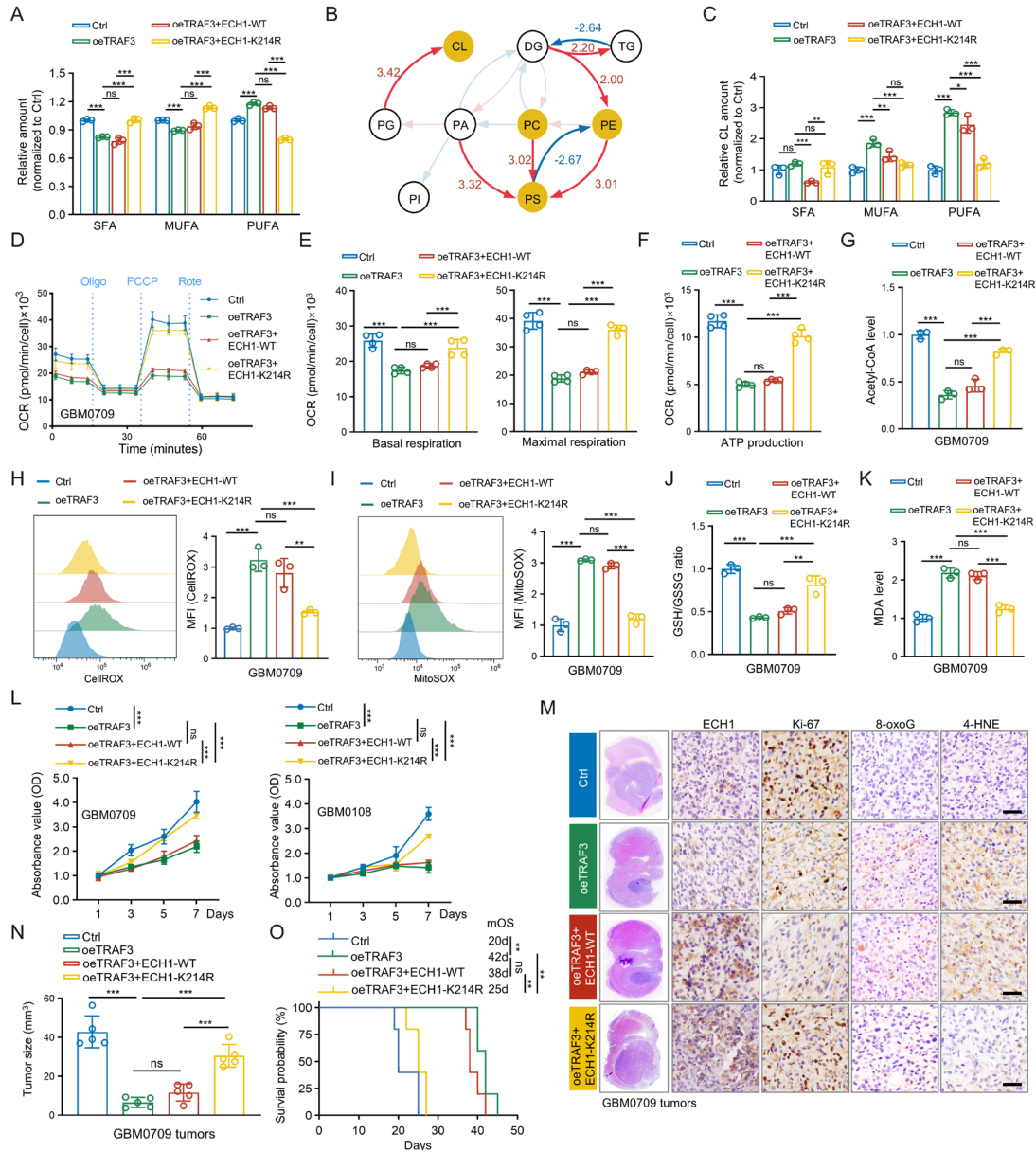
**Figure 7. TRAF3 impedes FAO and induces lipid peroxidation in GBM cells through ubiquitination of ECH1.**

**(A)** Lipidomic analysis demonstrated the relative content of SFAs, MUFAs, and PUFAs in GBM0709 cells expressing TRAF3, TRAF3+ECH1-WT, or TRAF3+ECH1-K214R (mean ± SD, n=3 independent experiments). ns, not significant. ***P<0.001.

**(B)** Biosynthetic analysis of lipid species in GBM0709 cells expressing TRAF3 compared to the control group.

**(C)** Analysis of the content of SFAs, MUFAs, and PUFAs in CL in GBM0709 cells expressing TRAF3, TRAF3+ECH1-WT, or TRAF3+ECH1-K214R (mean ± SD, n=3 independent experiments). ns, not significant. *P<0.05, **P<0.01, ***P<0.001.

**(D)** Time series of OCR measurement in GBM0709 cells expressing TRAF3, TRAF3+ECH1-WT, or TRAF3+ECH1-K214R using the Seahorse Metabolic Analyzer.

**(E)** Quantification of basal respiration and maximum respiration in GBM0709 cells.

**(F)** Quantification of mitochondrial ATP production in GBM0709 cells.

**(G)** Quantification of acetyl-CoA levels in GBM0709 cells. From **(D)** to **(G)**, data were expressed as mean ± SD of n=3 or n=4 independent experiments. ns, not significant. ***P<0.001.

**(H** and **I)** Flow cytometry analysis of CellROX **(H)** and MitoSOX staining **(I)** in GBM0709 cells expressing TRAF3, TRAF3+ECH1-WT, or TRAF3+ECH1-K214R. Representative flow cytometry plots were shown The MFI was quantified (mean ± SD, n=3 independent experiments). ns, not significant. **P<0.01, ***P<0.001.

**(J)** GSH/GSSG ratios were evaluated in GBM0709 cells expressing TRAF3, TRAF3+ECH1-WT, or TRAF3+ECH1-K214R.

**(K)** The levels of MDA were detected in GBM0709 cells expressing TRAF3, TRAF3+ECH1-WT, or TRAF3+ECH1-K214R. In **(J)** and **(K)**, data were expressed as mean ± SD of n=3 independent experiments. ns, not significant. **P<0.01, ***P<0.001.

**(L)** Cell viabilities of GBM0709 and GBM0108 cells stably expressing TRAF3, TRAF3+ECH1-WT, or TRAF3+ECH1-K214R were evaluated by CCK8. The

absorbance values were normalized to control (mean ± SD, n=4 independent assays). ns, not significant. ***P<0.001.

**(M** and **N)** GBM0709 cells stably expressing TRAF3, TRAF3+ECH1-WT, or TRAF3+ECH1-K214R were intracranially injected into nude mice. H&E-stained sections show representative tumor xenografts **(M)**. Mouse tumor tissues were stained with ECH1, Ki-67, 8-oxoG, and 4-HNE, respectively **(M)**. Scale bar, 100 μm. Tumor volumes were calculated **(N)**. (mean ± SD, n=5 mice for each group). ns, not significant. ***P<0.001.

**(O)** The survival of the GBM0709 GBM-bearing mice was evaluated (n=5 mice for each group, Kaplan-Meier model). ns, not significant. **P<0.01. Statistical analysis was performed using one-way ANOVA with Tukey post hoc test (A, C, E, F, G, H, I, J, K, L, and N), or Log-rank test (O).
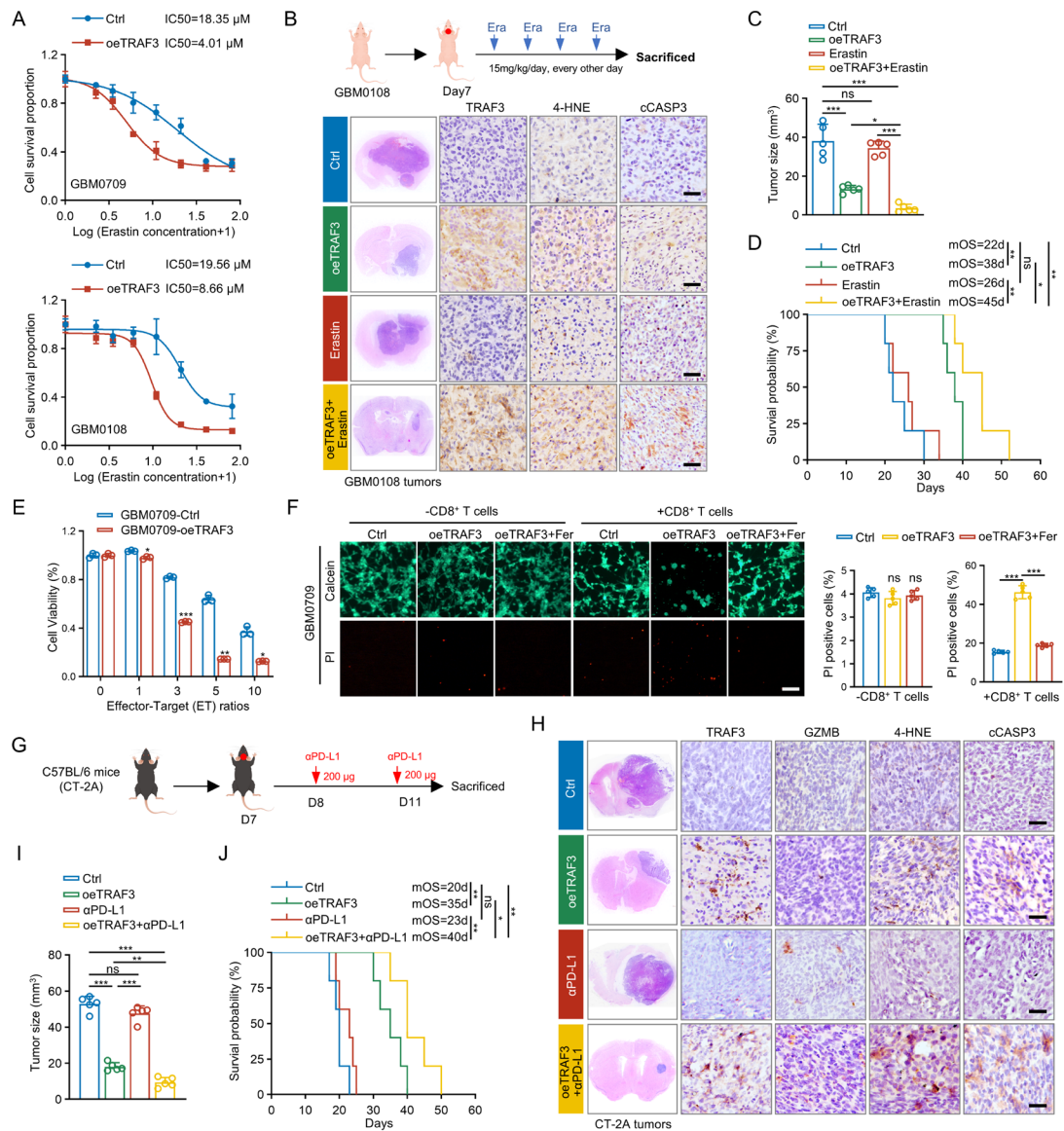
**Figure 8. Overexpression of TRAF3 sensitizes GBM to erastin and anti-PD-L1 therapy.**

**(A)** GBM0709 and GBM0108 cells expressing TRAF3 were treated with different concentration of erastin for 72 h. IC$_{50}$ values for each cell lines were calculated (mean ± SD, n=4 independent experiments).

**(B and C)** GBM0108 cells ($5\times10^5$ cells/mouse) stably expressing TRAF3 were intracranially injected into nude mice. Mice were then intraperitoneally injected with erastin (15 mg/kg/d) every other day. H&E-stained sections show representative tumor

xenografts **(B)**. The mouse tumor tissues were stained with TRAF3, 4-HNE, and cleaved-CASP3, respectively **(B)**. Scale bars, 100 μm. Tumor volumes were calculated **(C)** (mean $\pm$ SD, n =5 mice for each group). ns, not significant. *P<0.05, ***P<0.001.

**(D)** The survival of mice was evaluated (n=5 mice for each group, Kaplan-Meier model). ns, not significant. *P<0.05, **P<0.01.

**(E)** GBM0709 cells expressing TRAF3 were co-cultured with activated CD8$^+$ T cells for 48h with different effector-target (E:T) ratios (from 1:1 to 10:1). Cell viabilities were evaluated (mean $\pm$ SD, n=3 independent experiments). *P<0.05, **P<0.01, ***P<0.001.

**(F)** GBM0709 cells expressing TRAF3 were treated with Ferrostatin or DMSO and then co-cultured with activated CD8$^+$ T cells for 48h (E-T ratio=3:1). The surviving and dead cells were stained by Calcein-AM/PI. Representative images were shown. Scale bar, 100 μm. The percentage of PI positive cells were counted (mean $\pm$ SD, n=5 randomly selected microscope fields). ns, not significant. ***P<0.001.

**(G-I)** CT-2A cells stably expressing *TRAF3* were intracranially injected into C57BL/6 mice. Mice were then intraperitoneally injected with PD-L1 mAb (200 μg/mouse/d) for two times **(G)**. H&E-stained sections show representative tumor xenografts **(H)**. The mouse tumor tissues were stained with TRAF3, GZMB, 4-HNE, and cleaved-CASP3, respectively **(H)**. Scale bars, 100 μm. Tumor volumes were calculated **(I)** (mean $\pm$ SD, n=5 mice for each group). ns, not significant. **P<0.01, ***P<0.001.

**(J)** The survival of the CT-2A GBM-bearing mice was evaluated (n=5 mice for each group, Kaplan-Meier model). ns, not significant. *P<0.05, **P<0.01. Statistical

analysis was performed using one-way ANOVA with Tukey post hoc test (C, E, F, and

I) or Log-rank test (D and J).